Relativistic effects in the deuteron and processes of its fragmentation in interaction with the nucleon

G. I. Lykasov
Joint Institute for Nuclear Research, Dubna

Fiz. Elem. Chastits At. Yadra **24**, 140–179 (January–February 1993)

A review is given of relativistic effects in the deuteron, its interaction with nucleons at high and intermediate energies, and also quark effects. Weinberg's light-cone diagrammatic technique is briefly presented. An analysis of dN interactions is made in the framework of this approach, and deuteron fragmentation and hard NN scattering in pd interactions are considered. The theory is compared with experiment, and predictions for new experiments are made.

INTRODUCTION

The investigation of the interaction of deuterons with nucleons and nuclei at high energies has recently become very topical. There is particular interest in processes that would yield additional information on the deuteron structure. These are processes of deuteron fragmentation on different targets, i.e., the stripping reactions $dN \to pX$, $dA \to pX$,[1-3] hard scattering,[4-7] and the production of hadrons h in the processes $Nd \to hX$ in the kinematic region forbidden for the reaction $NN \to hX$ on the free nucleon, the so-called cumulative processes.[1,4,8] For the same reason, studies are also made of elastic and quasielastic[9,10] ed scattering, deep inelastic ed interactions,[11,12] etc.

Investigating such processes in the kinematic region corresponding to small intradeuteron distances, the authors of many studies attempted to extract information about the deuteron quark structure by comparing theoretical calculations with experimental data. There exist several approaches to the description of the deuteron quark structure.[2,13,14] A nonrelativistic, so-called hybrid model[14] is quite often used to take into account the six-quark state of the deuteron. However, as was shown in Refs. 13, 15, and 17, relativistic effects are extremely important, particularly at short intradeuteron distances,[17] although there does not yet exist a definite procedure for making the deuteron wave function relativistic. The question then arises of the validity of the description of the experimental data and new predictions obtained in the hybrid quark model if the deuteron quark structure is studied in the framework of a nonrelativistic potential approach.[14]

In addition, the deuteron structure at short intradeuteron distances was investigated in Refs. 16, 18, and 19 in the simplest pole approximation or even using the spectator mechanism to analyze the above processes. However, as was shown in Refs. 20–23, the pole approximation and, *a fortiori*, the spectator mechanism alone are inadequate in an investigation of Nd and ed processes, since in certain kinematic regions the contributions of the nonpole nonspectator graphs are quite important.

Therefore, in this review we analyze the role of these very important phenomena in the investigation of dN interactions at intermediate and high energies, namely, we consider relativistic effects in the deuteron and the mechanism of the dN reaction. The relativistic effects in the deuteron are considered in this review in the framework of established approaches proposed earlier by various authors (Refs. 13, 15, 16, 18, 19, 24, and 25). To analyze the mechanism of the dN interaction at high energies, we propose the approach of Ref. 17, which is based on Weinberg's diagrammatic technique in the infinite-momentum frame[26-28] and takes into account relativization of the deuteron wave function. An advantage of such a treatment compared with others is that, on the one hand, it enables one to obtain an expression for the amplitude of the dN process that depends explicitly only on relativistically invariant variables, while, on the other hand, such an approach is technically simpler in the calculation of the matrix elements of dN reactions compared with the calculation of Feynman diagrams.

The review is arranged as follows. Section 1 gives a brief review of different methods of making the deuteron wave function relativistic, particular attention being devoted to the covariant approach proposed by Karmanov.[15] Section 2 presents the essence of Weinberg's diagrammatic technique[27,28] and its application to the analysis of deuteron–nucleon processes. Section 3 considers specific dN interactions: a) deuteron fragmentation $dN \to pX$; b) "hard" dN scattering.

We give the results of calculations of various observable quantities, including polarization characteristics, compare the theory and experiment, and give new predictions. Section 4 considers one of the approaches to the investigation of non-nucleon degrees of freedom in the deuteron. Finally, in Sec. 5 the main conclusions are drawn from the material presented in the previous sections, and the importance of investigating dN processes in the kinematic region corresponding to short intradeuteron distances is demonstrated. The prospects for theoretical and experimental investigation of the deuteron structure are discussed.

1. RELATIVISTIC EFFECTS IN THE DEUTERON

In this section, we wish to present briefly two approaches (Refs. 13, 15, 16, 18, and 19) to the problem of relativization of the deuteron wave function. We first at-

 1063-7796/93/010059-18$10.00

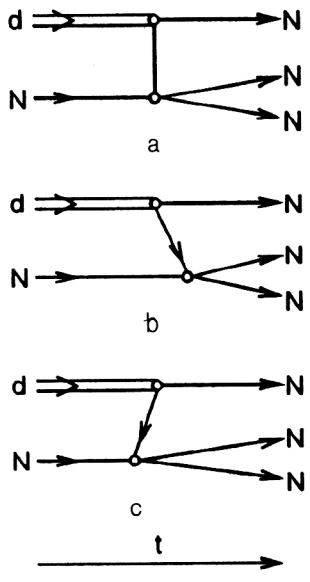

FIG. 1. Feynman diagrams of the process $dN \to NNN$ and equivalent graphs of the old perturbation theory.

tempt, on the basis of the studies mentioned above, to understand which variables must be the argument of the wave function.

In the general relativistic case, the deuteron vertex dNN does not reduce merely to dissociation of the deuteron into two nucleons; it may also include annihilation $\bar{N}d \to NN$, and therefore the deuteron decay vertex cannot always be reduced to an ordinary deuteron wave function whose square is the probability of finding a nucleon in the deuteron with definite momentum. As is well known, a Feynman graph of nth order is equivalent to $n!$ time-ordered graphs of the old perturbation theory. If dN processes are considered in the infinite-momentum frame, then many graphs in the old perturbation theory make a contribution of order $1/P$, where P is the total momentum of the incident particles, and therefore in the limit $P \to \infty$ they can be ignored. There remain only the diagrams that correspond to dissociation of the deuteron into two nucleons.[27-29]

As an example, Fig. 1 gives the Feynman diagram of the process $dN \to NNN$ (Fig. 1a) and the two equivalent diagrams of the old perturbation theory, ordered in the time t (Figs. 1b and 1c).

The diagram of Fig. 1c behaves as $1/P^2$ if the NN vertex does not depend on the spin,[27-29] i.e., decreases with increasing P. But if the spin dependence of the NN interaction is taken into account, then the contribution of the diagram will decrease as $1/P$.[27-29]

Therefore, one can introduce the concept of a deuteron wave function with the usual probability interpretation. However, what are the variables on which it must depend? In accordance with Refs. 18, 19, and 30, Ψ depends on

$$k^2 = \frac{m_\perp^2}{4x(1-x)} - m^2,$$

where x is a light-cone variable and is related to the momentum q of the spectator proton emitted backward in the deuteron rest frame (the spectator nucleon corresponds to the line emanating from the upper vertex of the diagram in Fig. 1a or Fig. 1b) as follows (Refs. 8 and 13): $x=(E(q)+q)/(2m)$, where $E(q)=(q^2+m^2)^{1/2}$ is the energy of the spectator proton; $m_\perp^2 = k_\perp^2 + m^2$; $k_\perp$ and m are the transverse momentum and mass of the intradeuteron nucleon. The variable k^2 is proportional to the difference of the energies in the dNN vertex in the diagram of Fig. 1b, as was noted in Ref. 30, i.e., $k^2 \sim P\Delta E$, where $\Delta E = E(p_d) - E(k_1) - E(k_2)$. The last relation is readily obtained by expressing the momenta of the incident deuteron, p_d, and of the intradeuteron nucleons, k_1 and k_2, in the infinite-momentum frame:

$$\begin{aligned} &p_d(P + M_d^2/2P, O_\perp, P); \\ &k_1\left(xP + \frac{m_\perp^2}{2xP}, k_\perp, xP\right); \\ &k_2\left[(1-x)P + \frac{m_\perp^2}{2(1-x)P}, -k_\perp, (1-x)P\right]. \end{aligned} \tag{1}$$

We recall that in each vertex of a diagram in the old perturbation theory, for example, in Figs. 1b and 1c, the 3-momentum is conserved but the energy is not, although the energy and 3-momentum are conserved for the complete reaction. At the same time, all particles, including those in an intermediate state, are on the mass shell. In the Feynman-diagram technique the 4-momentum is conserved at each vertex of a diagram, for example, in Fig. 1a, but the intermediate particle with 4-momentum k_N is off the mass shell, i.e., $k_N^2 \neq m^2$, where m is the mass of the particle.

In such an approach,[18,19] the deuteron wave function Ψ is related to the nonrelativistic deuteron wave function $\Phi_{\text{n.r.}}$, which, however, depends on the relativistically invariant variable k^2:

$$\Psi(x, k_\perp) = \left(\frac{m_\perp^2}{4x(1-x)}\right)^{1/4} \Phi_{\text{n.r.}}(k^2). \tag{2}$$

At the same time, Ψ is normalized as follows:

$$\frac{1}{2}\int_0^1 \frac{dx}{x(1-x)} \int |\Psi(x, k_\perp)|^2 d^2k_\perp = 1. \tag{3}$$

There is a different, covariant approach to relativization of the deuteron wave function; it was proposed in Ref. 15 and is based on a three-dimensional formulation of quantum field theory.[26] In it, not only the 3-momentum but also the energy is conserved in deuteron disintegration (see Fig. 1b), i.e., the 4-momentum is conserved at the dNN vertex: $k_1 + k_2 = p_d + \omega\tau$, where τ is some nonvanishing parameter, and the four-vector ω determines the surface of the light front. At the same time, all the nucleons are on the mass shell, i.e., $k_N^2 = m^2$. The dNN vertex with energy–momentum conservation is shown graphically in Fig. 2.[15] The broken line corresponds to a certain fictitious particle—the so-called spurion, which was first introduced by Kadyshevskiĭ.[26] Figure 2 shows graphically the so-

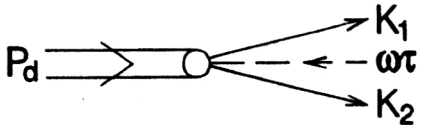

FIG. 2. The *dNN* vertex.

called four-leg diagram corresponding to the amplitude of the binary reaction $1+2\to 3+4$. Then the wave function of a bound system, in particular the deuteron, $\Psi(k_1,k_2,P,\omega\tau)$, can be constructed in the same way as this "four-leg" amplitude. Such a construction of the wave function can be done in the approach proposed in Ref. 15. In the simplest case of spinless particles forming a bound system with total momentum equal to zero, the wave function, like the amplitude of the binary reaction shown in Fig. 2, depends on two relativistically invariant variables:[15]

$$s_1=(k_1+k_2)^2=(p_d+\omega\tau)^2;\quad t_1=(p_d-k_1)^2,$$

where $\Psi=\Psi(s_1,t_1)$. In an equivalent form, this wave function also depends on the variables $\vec{q}^2$, $\vec{q}\vec{n}$, i.e., $\Psi=\Psi(\vec{q}^2,\vec{q}\vec{n})$, where $\vec{q}$ is the 3-momentum of one of the nucleons in their center-of-mass system, in which $\vec{k}_1+\vec{k}_2=0$;

$$q^2=\frac{1}{4}s_1-m^2=\frac{m_1^2}{4x(1-x)}-m^2;$$

$$\vec{q}\vec{n}=(2m^2+M_d^2-s_1-2t_1)\sqrt{s_1}/(2s_1-M_d^2);$$

$$\vec{n}=\vec{\omega}/\omega_0.$$

If a definite direction of the infinite-momentum frame is chosen, for example, $\vec{p}_d\uparrow\downarrow\vec{n}$, then the deuteron wave function will depend on the same variable k^2 considered above, as in the methods of Refs. 18 and 19.

In the general case with spin, the deuteron wave function on the light cone has, as was shown in Ref. 15, a more complicated structure than the nonrelativistic deuteron wave function, namely, instead of the two S and D waves, it is determined by six relativistically invariant functions. The number of functions is increased because the vector $\vec{n}$ occurs in the construction of the deuteron angular momentum on an equal footing with the momentum q.[15] However, if we consider deuteron fragmentation in the forward direction, the distinguished direction corresponding to the vector $\vec{n}$ loses its meaning,[15] and the deuteron wave function Ψ will again be determined by S and D waves, i.e., it will have the same spin structure as in the nonrelativistic case.

We briefly present one further method of taking into account relativistic effects in the deuteron,[16] which in what follows we shall also use in the analysis of $dN\to pX$ stripping in order to compare it with the methods of Refs. 13, 15, 18, 19, and 25. In this method, the *dNN* vertex (see Fig. 1a) is decomposed with respect to the invariants:[16]

$$\Gamma_\alpha=k_\alpha[a_1+a_2(m+\hat{k}_1)]+\gamma_\alpha[a_3+a_4(m+\hat{k}_1)],$$

where $\hat{k}_1=k_{1\beta}\gamma_\beta$, and k and k_1 are the 4-momenta of a real, i.e., $k^2=m^2$, and virtual, $k_1^2\neq m^2$, nucleon of the deuteron, respectively; γ_α are the components of the Dirac matrices. In this approach, as can be seen from the expression for the vertex Γ_α, one nucleon is on the mass shell (with 4-momentum k), while the other is off the mass shell and virtual (with momentum k_1).

There are some other methods for taking into account relativistic effects in the deuteron: a) the method based on solution of Bethe–Salpeter equations (Ref. 31); b) the so-called dispersion method,[32] based on the technique of dispersion relations; c) the Lagrange method on the light cone considered in Refs. 33 and 34.

2. WEINBERG'S DIAGRAMMATIC TECHNIQUE AND ITS APPLICATION TO THE *dN* INTERACTION

Weinberg's formalism

As we have already noted, in the infinite-momentum frame it is convenient to use the old perturbation theory in the analysis of the interaction of particles with composite systems. This is the case because many time-ordered diagrams decrease as $1/P$, and they can be ignored at large P. The calculation of the scattering amplitudes is greatly simplified compared with calculations of Feynman diagrams. The diagrammatic technique in the infinite-momentum frame was first proposed by Weinberg[27] in 1966. It is readily understood if one recalls the connection between Feynman diagrams and time-ordered graphs of the old perturbation theory. As an example, we consider an interaction of spinless particles of the type φ^3. The matrix element of such an interaction can be calculated in accordance with the following rules:[27,28]

1. In a Feynman graph of nth order, each vertex i is associated with an interaction time t_i. One then draws all $n!$ graphs corresponding to all permutations of the times (and, accordingly, i vertices). As an example, Fig. 3 shows a Feynman graph of third order in the coupling constant g corresponding to six graphs of the old perturbation theory ordered in the time t.

2. Each line of each time-ordered graph is associated with a 3-momentum p_i.

3. For each vertex, except the last, one writes down the factor $(2\pi)^3\delta^{(3)}(\Sigma_i p_i)$, where the δ function expresses the 3-momentum conservation at this vertex. For the last factor, one writes down only the factor g, and it is not necessary to take into account the conservation law at this vertex, since that is done by the conservation law of the total energy and total momentum of the complete process.

4. Each internal line is associated with the factor $(2\pi)^{-3}(2E_i)^{-1}$, where E_i is the energy of the particle corresponding to this line and is on the mass shell, i.e.,

$$E_i^2=p_i^2+m^2.$$

5. For each intermediate state, i.e., state between the interaction times t_i and t_j (Fig. 3 shows vertical broken lines separating these times) the following Green's function is determined:

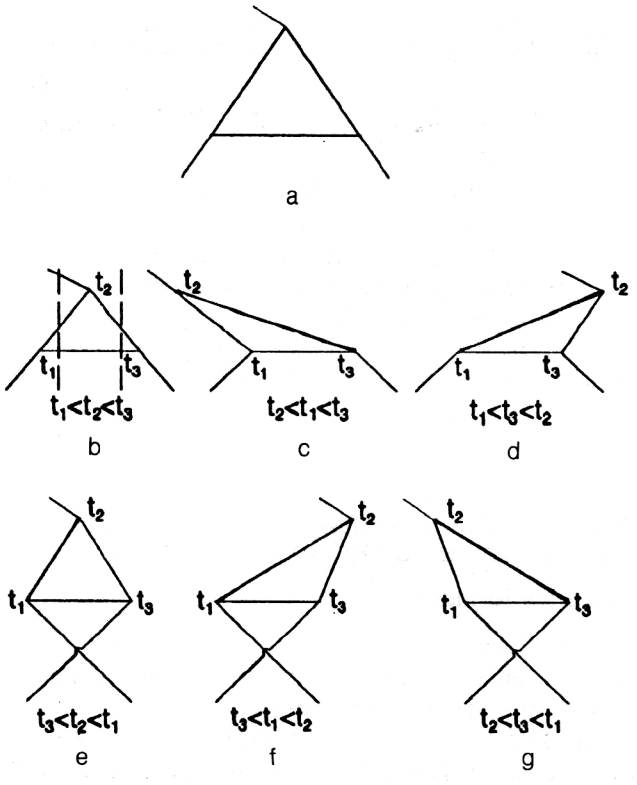

FIG. 3. Feynman graph of third order (a) in the coupling constant g and corresponding time-ordered diagrams of the old perturbation theory (b–g).

$$G=\frac{1}{E_{\text{inc}}-E_{\text{int}}+i\varepsilon}; \tag{4}$$

where E_{inc} is the total energy of the incoming particles, and E_{int} is the sum of the energies of the particles in the intermediate state (for example, between the vertical broken lines in Fig. 3).

6. Integration is performed over all internal lines, i.e., over d^3p_i.

7. All the time-ordered graphs are added together.

Note that the sum of all such graphs of the old perturbation theory give a Feynman diagram of the given nth order, for example, the third, as in Fig. 3, that does not depend on the frame of reference, although each of them does depend on the choice of the frame.

In the infinite-momentum frame, the above rules for calculating the matrix element of a process can be expressed in a form that depends on invariant variables, the light-cone variable x and $k_\perp$. We shall observe a scattering process from, for example, a system moving with high velocity along the negative z axis; then the total initial momentum P will also be large but directed along the positive z axis (as in Fig. 2). It is easy to show that in such a system in the limit $P\to\infty$ each time-ordered graph either has a finite value or decreases and in the limit is equal to zero.

Each three-momentum corresponding to the ith line can be represented in the infinite-momentum frame as in Sec. 1 in the form

$$p_i=x_iP+k_{i\perp},$$

where x_i is the fraction of the total momentum P, $k_{i\perp}$ is the transverse momentum of the ith particle,

$$\sum_{\text{inc}} p_i=P;\quad \sum_{\text{inc}} x_i=1;\quad \sum_{\text{inc}} k_{i\perp}=0.$$

The same relations also hold for the sums over the intermediate states from the law of conservation of the 3-momentum at the vertices, i.e.,

$$\sum_{\text{int}} x_i=1;\quad \sum_{\text{int}} k_{i\perp}=0.$$

In the limit $P\to\infty$, the energy of the ith particle can be represented in the form

$$E_i=(p_i^2+m^2)^{1/2}\cong|x_i|P+\frac{m_{i\perp}^2}{2x_iP}.$$

Using these relations, we readily obtain

$$E_{\text{inc}}=\sum_{\text{inc}} E_i\cong P+\sum_{\text{inc}}\frac{m_{i\perp}^2}{2x_iP}=P+\sum\frac{s_i}{2P},$$

$$E_{\text{int}}=\sum_{\text{int}} E_i\cong P+\sum_{\text{int}}\frac{m_{i\perp}^2}{2x_iP}=P+\sum\frac{s_i}{2P},$$

$$s_i=m_{i\perp}^2/x_i.$$

Hence, for the Green's function G we have

$$G=\frac{1}{E_{\text{inc}}-E_{\text{int}}+i\varepsilon}=\frac{2}{\Sigma_{\text{inc}}s_i/P-\Sigma_{\text{int}}s_i/P+i\varepsilon}$$

for intermediate states with $x_i>0$, and

$$G=\frac{1}{E_{\text{inc}}-E_{\text{int}}+i\varepsilon}=\frac{1}{2\Sigma_{x_i<0}x_iP+i\varepsilon}$$

for intermediate states with $x_i<0$.

Note that for all external particles (see, for example, Fig. 3) $x_i>0$, and there will be $n-1$ Green's functions G in the old perturbation theory, since there are $n-1$ intermediate states. But the conservation laws for the 3-momenta at the vertices are now expressed in the form

$$\delta^{(3)}\Big(\sum_i p_i\Big)=\delta\Big[\Big(\sum_i x_i\Big)P\Big]\delta^{(2)}\Big(\sum_i k_{i\perp}\Big)$$
$$=\frac{1}{P}\delta\Big(\sum_i x_i\Big)\delta^{(2)}\Big(\sum_i k_{i\perp}\Big),$$

and since the number of δ functions is $n-1$, we obtain the factor $P^{-(n-1)}$. The integration over the internal momenta is now expressed as

$$\frac{d^3p_i}{(2\pi)^3 2E_i}=\frac{dx_i d^2k_{i\perp}}{2|x_i|(2\pi)^3}.$$

It can be seen from the above that for intermediate states with $x_i>0$ the time-ordered diagrams give a finite value. For $x_i<0$, they decrease as $1/P^n$. Thus, the number of time-ordered diagrams that make the main contribution becomes much less than $n!$ (Ref. 27). If we now, for example, consider the interaction of a photon with the deu-

teron, i.e., for the upper external line in Fig. 3 we consider a photon γ and for the lower external lines a deuteron, then for the choice of the infinite-momentum frame in which the photon 4-momentum has the components

$$q(M\nu/2P,\ q_\perp\ ,0)$$

(ν is the energy of the photon, $q_\perp$ is its transverse momentum, and M is the deuteron mass) we have in place of the six time-ordered diagrams just one, corresponding to Fig. 3a, which remains finite.

We now briefly formulate the rules of Weinberg's diagrammatic technique that follow from the above.[27,28]

1′. In place of the Feynman graph of order n, we draw all time-ordered graphs in which each vertex has at least one line that emanates from the past and one line that goes into the future.

2′. Each line is associated with x and $k_\perp$.

3′. With each vertex except the last we associate a factor

$$(2\pi)^3 g\delta\Big(\sum_i x_i\Big)\delta^{(2)}\Big(\sum_i k_{i\perp}\Big),$$

and with the last vertex the factor g.

4′. For each intermediate state we determine the Green's function

$$G=\frac{2}{\Sigma_{\text{inc}}s_i-\Sigma_{\text{int}}s_i+i\varepsilon}.$$

5′. Over the internal lines we integrate with respect to

$$\frac{dx_i d^2k_{i\perp}\,\theta(x_i)}{(2\pi)^3 2x_i}.$$

6′. All the time-ordered graphs are added together.

All the above applies to the interaction of spinless particles. In the case of particles with spin, everything is somewhat more complicated, i.e., some vertices in diagrams of the type of Fig. 3 can behave as $\sim P$, i.e., increase with increasing P for $x_i<0$.[27] However, overall, such a time-ordered diagram can decrease, not as $1/P^n$, but as $1/P^{n-1}$ (Ref. 27). Quite generally, if the particles have spin, one must exercise care and verify which diagrams make a finite contribution.

We now apply Weinberg's approach to the analysis of dN interactions at high energies.

The dN interaction in the framework of Weinberg's formalism

For simplicity, we consider deuteron disintegration at high energies: $dp\to ppn$. Let P be the total momentum of the initial particles, and x_N and x_d be the fractions of the longitudinal momenta from the initial nucleon and initial deuteron, respectively; x_1, x_2, x_3 are the fractions of the longitudinal momenta of the proton, neutron, and detected proton:

$$s_d=\frac{M^2}{x_d};\quad s_N=\frac{m^2}{x_N};\quad s_1=\frac{m^2+p_{1\perp}^2}{x_1};$$

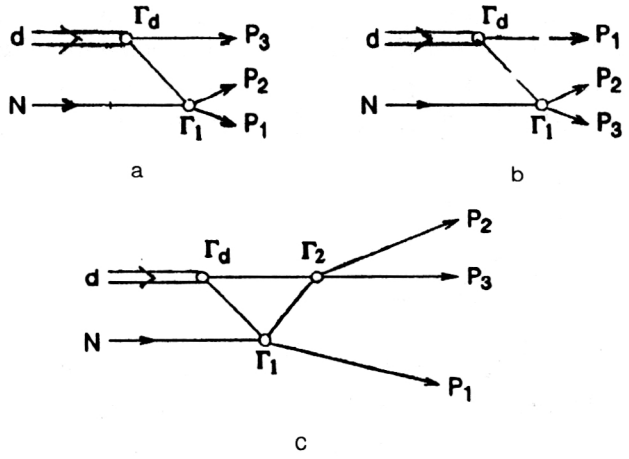

FIG. 4. Some diagrams of the process $dp\to ppn$.

$$s_2=\frac{m^2+p_{2\perp}^2}{x_2};\quad s_3=\frac{m^2+p_{3\perp}^2}{x_3},$$

where $p_{1\perp}$, $p_{3\perp}$, and $p_{2\perp}$ are the transverse momenta of the emitted protons and neutron, and m and M are the nucleon and deuteron masses, respectively. We consider the diagrams of this process up to second order in the hN interaction (see Fig. 4) in the framework of Weinberg's formalism[26] in the infinite-momentum frame. We fix a definite direction of the frame, for example, $\vec{n}\uparrow\downarrow-\vec{P}$, and then the deuteron wave function will depend only on k^2 or on x and $k_\perp$.[15,22]

In accordance with the above rules, the amplitude corresponding to the pole graph (Fig. 4a) can be written as follows:

$$\begin{aligned}F^{(1)}&=\int(2\pi)^3\Gamma_d\delta(x_d-x^3-x_3)\delta^{(2)}(k'_\perp+k_{3\perp})\\&\quad\times\frac{2\Gamma_1}{s_d-s'-s_3+i\varepsilon}\frac{dx'\theta(x')d^2k_\perp}{(2\pi)^3 2x'2x_3}\\&=\frac{\Gamma_d}{s_d-s'-s_3+i\varepsilon}\frac{\Gamma_1}{2x_3(1-x_3)}\\&=f_{1,NN}\frac{\Psi(x_3,P_{3\perp})}{\sqrt{2x_3(1-x_3)}}.\end{aligned}\tag{5}$$

In (5), we have gone over from Γ_1 to the NN scattering amplitude $f_{1,NN}$, and from Γ_d to the deuteron wave function $\Psi(x_3,P_{3\perp})$:

$$\Psi(x_3,P_{3\perp})=\frac{\Gamma_d}{(s_d-s'-s_3+i\varepsilon)\sqrt{2x_3(1-x_3)}},$$

which is normalized by the condition (3). The amplitude corresponding to the second pole graph (Fig. 4b) has the similar form

$$F^{(2)}=f_{2,NN}\frac{\Psi(x_1,p_{1\perp})}{\sqrt{2x_1(1-x_1)}}.\tag{6}$$

We now consider the diagrams of the following, i.e., second, order in the hN interaction in this formalism (Fig. 4c). In accordance with the above rules, we have for the amplitude $F^{(3)}$ corresponding to the graph of Fig. 4c

$$F^{(3)}=\int (2\pi)^3\Gamma_d\delta(x_d-x'-x_3')\delta^{(2)}(k_{1\perp}+k_{3\perp})$$
$$\times\frac{2}{s_d-s_1'-s_3'+i\varepsilon}(2\pi)^3\Gamma_1\delta(x_N+x_1'-x_1-x_2')$$
$$\times\delta^{(2)}(k_{1\perp}-k_{2\perp}-p_{1\perp})\frac{2}{s_1'+s_N-s_1-s_2'+i\varepsilon}$$
$$\times\Gamma_2\frac{dx_1'\theta(x_i')d^2k_{1\perp}\,dx_2'\theta(x_2')d^2k_{2\perp}\,dx_3d^2k_{3\perp}}{(2\pi)^3 2x_1'(2\pi)^3 2x_2'(2\pi)^3 2x_3'}. \quad (7)$$

Going over now in (7) from the vertices Γ_d, Γ_1, Γ_2 to the deuteron wave function and to the amplitudes of the hN interaction, we have for $F^{(3)}$ the expression

$$F^{(3)}=\frac{1}{(2\pi)^3}\int\Psi(x_1',k_{1\perp})f_{1,NN}f_{2,NN}$$
$$\times\frac{\tilde{G}(x_1',k_{1\perp})}{4\sqrt{x_1'(1-x_1')x_2'}}dx_1'd^2k_{1\perp};\quad \tilde{G}=\frac{1}{P}G;$$
$$G=\frac{2P}{s_1'+s_N-s_1-s_2+i\varepsilon}$$
$$\equiv\frac{1}{E(k_1)+E(p_N)-E(p_1)-E(q)+i\varepsilon};$$
$$x_2'=x_1'+x_N-x_1. \quad (8)$$

We can rewrite $F^{(3)}$ in the equivalent form[17,35]

$$F^{(3)}=\frac{P}{(2\pi)^3}\int\frac{f_{1,NN}f_{2,RN}dx_1'd^2k_{1\perp}}{4\sqrt{E(k_1)E(k_2)E(q)}}$$
$$\times\Psi(x_1',k_{1\perp})G(x_1',k_{1\perp}). \quad (9)$$

Note that as the intermediate particle R with momentum q in the graph of Fig. 4c we may have not only a nucleon but, for example, a baryon resonance.[17,35] Therefore, we shall denote the amplitude corresponding to the interaction of this particle with the nucleon by $f_{2,RN}$. It can be seen from (6) and (8) that the amplitudes of the considered diagrams do not depend explicitly on the initial momentum P but depend only on the relativistically invariant variables x and $k_\perp$.

We now consider how the differential cross section for the process is expressed in such variables:

$$d\sigma=\frac{(2\pi)^4\delta(E_{\text{in}}-E_f)\delta^{(3)}(p_{\text{in}}-p_f)}{2\lambda^{1/2}(s_{pd},m^2,M^2)}|F|^2$$
$$\times\frac{d^3p_1}{(2\pi)^3 2E_1}\frac{d^3p_2}{(2\pi)^3 2E_2}\frac{d^3p_2}{(2\pi)^3 2E_3}, \quad (10)$$

where $\lambda^{1/2}(x,y,z)=[(x-y-z)^2-4yz]^{1/2}$, and F is the amplitude of the considered $dp\to ppn$ reaction. Taking into account (10), we have the invariant spectrum of protons with momentum p_3:

$$E_3\frac{d\sigma}{d^3p_3}=\frac{1}{16\lambda^{1/2}(s_{pd},m^2,M^2)}\frac{1}{(2\pi)^5}\delta(E_{\text{in}}-E_f)$$
$$\times\delta^{(3)}(p_{\text{in}}-p_f)|F|^2\frac{d^3p_1d^3p_2}{E_1E_2}$$
$$=\frac{1}{16\lambda^{1/2}(s_{pd},m^2,M^2)}\frac{1}{(2\pi)^5}$$
$$\times\int\delta(x_N+x_d-x_1-x_2-x_3)$$
$$\times\delta(s_d+s_N-s_1-s_2-s_3)|F|^2\frac{dx_1dx_2d^2p_\perp}{x_1x_2}. \quad (11)$$

If, to simplify the calculations, we assume azimuthal symmetry of the reaction, then in place of (11) we obtain

$$E_3\frac{d\sigma}{d^3p_3}=\frac{1}{16\lambda^{1/2}(s_{pd},m^2,M^2)}\frac{1}{(2\pi)^4}\int|F|^2\frac{dx_1}{1-x_3}$$
$$\times\delta(s_d+s_N-s_1-s_2-s_3)p_{1\perp}\,dp_{1\perp}. \quad (12)$$

It is fairly simple to integrate in (12) over $dp_{1\perp}$ in the case when one of the final nucleons, for example, the proton with momentum p_3, has zero transverse momentum, i.e., $p_{3\perp}=0$; then $s_3=m^2/x_3$, $p_{1\perp}^2=p_{2\perp}^2=p_1^2$, after which we obtain in place of (12) the expression

$$E_3\frac{d\sigma}{d^3p_3}=\frac{1}{16\lambda^{1/2}(s_{pd},m^2,M^2)}\frac{1}{(2\pi)^4}\int\frac{|F|^2dx_1}{1-x_3}. \quad (13)$$

We now consider specific dN interactions in the framework of Weinberg's approach.

3. THE dN INTERACTION

Deuteron fragmentation $dN\to pX$

We consider deuteron stripping on the nucleon, $dN\to pX$, when the proton is emitted forward or at an angle near 0° in the system of the moving deuteron, or backward, $\theta_p\approx 180°$, in the deuteron rest frame. We restrict ourselves to an analysis of the class of diagrams up to the second order in the hN interaction that can make an appreciable contribution, as was shown in a number of studies (Refs. 17, 21, 48, and 49), to the observable quantities of this reaction. These are the time-ordered diagrams of the old perturbation theory given in Fig. 5. In the case of simple deuteron disintegration, $dN\to NNN$, the remaining graphs will give a contribution that decrease with P, $\sim 1/P$, even if the spin structure in the vertices is taken into account.[28] In the case of the inclusive reaction $dN\to pX$, it is difficult to make a corresponding assertion, since the vertices Γ_1 and Γ_2 (see Fig. 5) will correspond to amplitudes of the inelastic NN interaction whose spin structure is, in the general case, unknown. However, as will be shown below, in certain cases the analysis of the inclusive dp reaction can

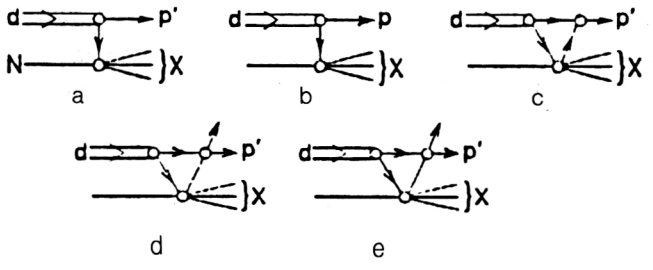

FIG. 5. Diagrams of the process $dp \to pX$.

be replaced by an equivalent consideration of the processes $dp \to NNN$, $dp \to NNN\pi$. The spin structure of the last two reactions is known, and the assertion can be proved in the same way as for deuteron disintegration.

The general expression for the amplitude of the process can be written in the form[17,35,36]

$$\mathcal{F}_d = C \sum_{i=1}^{5} \mathcal{F}^{(i)}, \tag{14}$$

where $C=(2(2\pi)^3)^{1/2}$ is a normalization factor,[17,35,36] and $\mathcal{F}^{(i)}$ correspond to the diagrams of Fig. 5.

Expressions for $\mathcal{F}^{(1)}, \mathcal{F}^{(2)}$ are given in the previous section [see Eqs. (5) and (6)]. The expressions for $\mathcal{F}^{(3)}, \mathcal{F}^{(4)}, \mathcal{F}^{(5)}$, corresponding to Figs. 5c–5e, will have a form analogous to (7)–(9). For the diagram of Fig. 5c, the vertex of absorption of an intermediate virtual meson by a nucleon has the form (Refs. 35 and 36) $\Gamma_N^{(2)} = ag\bar{u}(p')\gamma_5 u(k_1)$, where $a=\sqrt{2}$, $g^2/4\pi = 14.7$ for the π^+ meson and $a=1$ for the other pions. If the intradeuteron nucleons are near the mass shell, then

$$\bar{u}(p')\gamma_5 u(k_1) = b\zeta^+ \left\{ \frac{\sigma_N p'}{E'+m} - \frac{\sigma_N k_1}{E(k_1)+m} \right\} \zeta, \tag{15}$$

where

$$b = \left\{ \frac{(E(k_1)+m)(E(p')+m)}{4m^2} \right\}^{1/2},$$

and ζ is a two-component nucleon spinor.

If the energy of the incident deuteron is not very high, for example, $E_d \approx 10$–20 GeV, then, as the experimental data of Refs. 37 and 38 show, the production of vector mesons at the lower vertex of the diagram of Fig. 5c is very weak compared with the production of pseudoscalar mesons. Therefore, we ignore the diagram of Fig. 5c with absorption of a virtual vector meson and retain only the diagram of Fig. 5c with absorption of a pseudoscalar meson by a nucleon. As was shown in Ref. 39, such diagrams make a significant contribution to the spectra of protons emitted forward in the $dp \to ppn$ reaction for initial deuteron momentum $p_d \approx 3.3$–4 GeV/c, at which the reaction $pN \to \pi NN$ (see the upper vertex in Fig. 5c) proceeds mainly through production of the Δ isobar in the intermediate state. At larger initial momenta p_d, the contribution of the Δ-isobar mechanism in the $pN \to \pi NN$ process steadily decreases with increasing p_d, but at $p_d \approx 10$ GeV/c it is still significant. Therefore, as was shown in Refs. 17, 35, and 36, diagrams of the type of Fig. 5c cannot be ignored in the analysis of dN stripping reactions at such initial momenta. In inclusive reactions of the stripping type $dp \to pX$, the contribution of the diagram of Fig. 5c is still significant in the kinematic region $0.5 < x < 0.8$ even for high initial energies E_d. This is the case because it is determined by the inclusive spectrum of the $pN \to \pi X$ process, which depends weakly on the initial energy.

Further, if we analyze the considered dN reaction at not too large energies, for example, at $E_d \approx 9$ GeV, at which there are experimental data,[3,41] then the mean multiplicity of the produced mesons, mainly pions, is small ($\langle n_\pi \rangle \cong 1.0$–$1.5$; Ref. 42). This means that in this process not more than one pion is, on the average, produced at the indicated initial energy. According to Ref. 20, in dP stripping at such energies the final pion is produced with the greatest probability in the first collision of a deuteron nucleon with a target nucleon (see the upper vertex of Fig. 5d). Therefore, as the $NN \to \pi X_1$, $NN \to NX_1$ amplitudes in Figs. 5c–5e we can consider the amplitudes of the following processes: $NN \to \pi NN$ for the diagrams of Figs. 5d and 5e, and $NN \to NN$ for the graph of Fig. 5e. Note that each graph of Figs. 5c–5e corresponds to a coherent sum of diagrams that take into account all possible isotopic states of the intermediate and final particles.

It is now easy to calculate the inclusive spectrum of protons produced by deuteron fragmentation. In our case, the transverse momentum of the protons is zero, $p_\perp = 0$, and we can therefore use the expression (13) for the spectrum and substitute in it the amplitude (14). Such expressions and calculations of the individual diagrams of Figs. 5a–5e and their interferences to the inclusive proton spectrum are given in Refs. 36 and 37, and therefore we shall not give them here. The amplitudes of the processes $NN \to \pi NN$ corresponding to the lower vertices of Figs. 5c–5e were calculated in the framework of Reggeized one-boson exchange,[43] and the amplitudes of $\pi N \to \pi N$ scattering (see the upper vertex of Fig. 5e) were calculated from a phase-shift analysis (see the references in Ref. 43) at characteristic pion energies $E_\pi \approx 0.15$–0.7 GeV. For the amplitudes of elastic NN scattering, the partial-wave analysis of Ref. 44 was used.

In the framework of Weinberg's diagrammatic technique, one can also calculate other observable quantities of the considered fragmentation reaction, for example, the tensor analyzing power $A = \sqrt{2}T_{20}$ and the polarization transfer κ. This is of undoubted interest in the study of few-nucleon correlations or of non-nucleon degrees of freedom in the deuteron.

We begin by considering the first polarization characteristic T_{20}. As was pointed out in Sec. 1, in the case of dp stripping the spin structure of the relativistic deuteron wave function can be represented in the same form as for the nonrelativistic wave function. For convenience, we consider these processes in the deuteron rest frame. The approach presented above is also valid in this frame, provided that the total initial momentum is sufficiently large.

The general expression for the deuteron density matrix can be written in the form[45-47]

$$\rho_d=\tfrac{1}{3}P_T\{1+\tfrac{3}{2}\vec{\mathcal{P}}\cdot\vec{S}-\tfrac{1}{2}\rho_{20}(3S_z^2-2)\}; \tag{16}$$

where $P_T=(3+\sigma_p\sigma_n)/4$ is the projection operator of the deuteron triplet state, $\vec{\mathcal{P}}$ is the polarization vector of the deuteron, ρ_{20} is its tensor polarization, $\vec{S}$ is the operator of the deuteron spin, and S_z is its projection onto the quantization axis z, which in the given case coincides with the direction of motion of the initial particles. The tensor analyzing power A of the deuteron is defined as follows:[45]

$$A=\frac{\sigma(m=+1)+\sigma(m=-1)-2\sigma(m=0)}{\sigma(m=+1)+\sigma(m=-1)+\sigma(m=0)}, \tag{17}$$

where $\sigma(m=\pm1,0)$ is the differential cross section of the reaction for pure deuteron spin states. It is also the expectation value of the spin-tensor operator[45,46] $\Omega_{20}=3S_z^2-2$, i.e., $A=\langle\Omega_{20}\rangle=\sqrt{2}T_{20}$. In accordance with the definition of the expectation value of an operator, in particular Ω_{20}, the expression for T_{20} can be represented in the form[46,47]

$$T_{20}=\frac{1}{\sqrt{2}}\frac{\int \mathrm{Tr}(\rho_d\mathcal{F}_d^+\Omega_{20}\mathcal{F}_d)\delta^{(4)}(p_{\mathrm{in}}-p_f)\Gamma}{\int \mathrm{Tr}(\rho_d\mathcal{F}_d^+\mathcal{F}_d)\delta^{(4)}(p_{\mathrm{in}}-p_f)\Gamma}, \tag{18}$$

where $\Gamma=d^3p_1d^3p_2d^3p_4...d^3p_n/(E_1E_2E_4...E_n)$.

In (18), there is an integration over all the momenta of the final particles except for the one p_3, which corresponds to the detected proton. Knowing the number n of particles in the final state, we can represent the expression (18) in a form analogous to (12) and (13). Such expressions are given in Ref. 35 for our particular case of dp stripping at not too large initial energies. If the deuteron has only tensor polarization, i.e., $\vec{\mathcal{P}}=0$, then in accordance with (35) and (36) we have

$$T_{20}=\frac{2\sqrt{2}\Psi_0(x)\Psi_2(x)-|\Psi_2(x)|^2+\tilde{R}_1(x)+\tilde{R}_2(x)}{\sqrt{2}\{|\Psi_0(x)|^2+|\Psi_2(x)|^2+R_1(x)+R_2(x)\}}. \tag{19}$$

Expressions for $\tilde{R}_1$, $\tilde{R}_2$, R_1, R_2 are given in Ref. 36; they correspond to allowance for all nonspectator graphs of Figs. 5c–5e. In the approximation of the spectator mechanism, i.e., with allowance for only the diagram of Fig. 5a, $\tilde{R}_1=\tilde{R}_2=R_1=R_2=0$, and the expression (19) acquires the form obtained for stripping $dp\to pX$ by Strokovsky.[3,41]

We now consider a different polarization characteristic—the polarization $\vec{\mathcal{P}}'$ of the final proton in the $dN\to pX$ reaction. The general expression for $\vec{\mathcal{P}}'\vec{n}$, where $\vec{n}$ is a unit vector perpendicular to the reaction plane, has the form[46,47]

$$\vec{\mathcal{P}}'\vec{n}=\frac{\int \mathrm{Tr}(\rho_d\mathcal{F}_d^+\vec{\sigma}\vec{n}\mathcal{F}_d)\Gamma}{\int \mathrm{Tr}(\rho_d\mathcal{F}_d^+\mathcal{F}_d)\Gamma}, \tag{20}$$

where $\vec{\sigma}$ are the Pauli matrices corresponding to the final proton in the reaction. In an experiment, it is customary to measure the so-called polarization transfer $\kappa=(\vec{\mathcal{P}}'\vec{n})/(\vec{\mathcal{P}}\vec{n})$.[41] The expression (20) can also be represented in a form analogous to (12) and (13).

In the simplest case of the spectator mechanism, the expression for κ has a form that was also obtained by Strokovsky:[41]

$$\kappa^{sp}=\frac{\Psi_0^2(x)-\frac{1}{\sqrt{2}}\Psi_0(x)\Psi_2(x)-\Psi_2^2(x)}{\{\Psi_0^2(x)+\Psi_2^2(x)\}\{1-\rho_{20}T_{20}^{sp}\}}. \tag{21}$$

In the case when the deuteron has only vector polarization, i.e., $\rho_{20}=0$,

$$\kappa^{sp}=1-\frac{1}{2\sqrt{2}}T_{20}^{sp}-\frac{9}{4(1+(\Psi_0/\Psi_2)^2)}. \tag{22}$$

Here and in (21), the superscript sp means that these quantities are calculated in the framework of the spectator mechanism. One can calculate T_{20}^{sp} in accordance with (19), setting $\tilde{R}_1=\tilde{R}_2=R_1=R_2=0$. It can be seen from (19) that if a restriction could be made to just the spectator mechanism, which is shown in Fig. 5a, then one could extract directly information on the S and D waves separately from experimental data on κ and T_{20}. Such an assumption was made in Ref. 41. However, as was shown in Refs. 17, 35, and 36, the contribution of the other, nonspectator graphs cannot be ignored, especially in an investigation of polarization characteristics.

With allowance for all graphs of Fig. 5, the expression for κ has the form

$$\kappa=\frac{\Psi_0^2(x)-\frac{1}{\sqrt{2}}\Psi_0(x)\Psi_2(x)-\Psi_2^2(x)+\tilde{R}_N+\tilde{R}_{\mathrm{abs}}+\tilde{R}_{\pi,rs}}{\Psi_0^2(x)+\Psi_2^2(x)+R_N+R_{\mathrm{abs}}+R_{\pi,rs}}. \tag{23}$$

Detailed expressions for $\tilde{R}_N$, $\tilde{R}_{\mathrm{abs}}$, $\tilde{R}_{\pi,rs}$, R_N, R_{abs}, $R_{\pi,rs}$ corresponding to the graphs of Figs. 5b, 5e, 5c, and 5d are given in Ref. 36.

We now discuss the results of the calculation of the observable quantities $Ed\sigma/d^3p$, T_{20}, κ in the fragmentation $dp\to pX$.[17,35,36]

The inclusive spectrum of the protons in $dp\to pX$ at $p_d\approx9$ GeV/c is shown in Fig. 6. The relative contributions of the diagrams of Fig. 5 are given in Fig. 7. It can be seen from these figures (especially from Fig. 7) that the total contribution of the diagrams, taking into account secondary interactions, i.e., the diagrams of Figs. 5c–5e, is quite significant at momentum $0.2\leqslant q\leqslant0.45$ GeV/c of the protons emitted backward in the deuteron rest frame, while for $q>0.45$ GeV/c they decrease steadily and can be ignored. It can be seen from Fig. 7 that the contribution of nucleon rescattering (Fig. 5e) can be destructive on account of its interference with other diagrams at small q, $q\leqslant0.2$ GeV/c, i.e., it reduces the differential cross section calculated in the impulse approximation. This comes about because of the so-called final-state interaction of two nucleons, which in our approach is taken into account by the diagram of Fig. 5e; for details on this, see Ref. 36. This was also noted in Ref. 49, in which relativistic effects in the deuteron were not taken into account. At larger q, the contribution of NN rescattering increases the values of the spectrum calculated in the impulse approximation. The

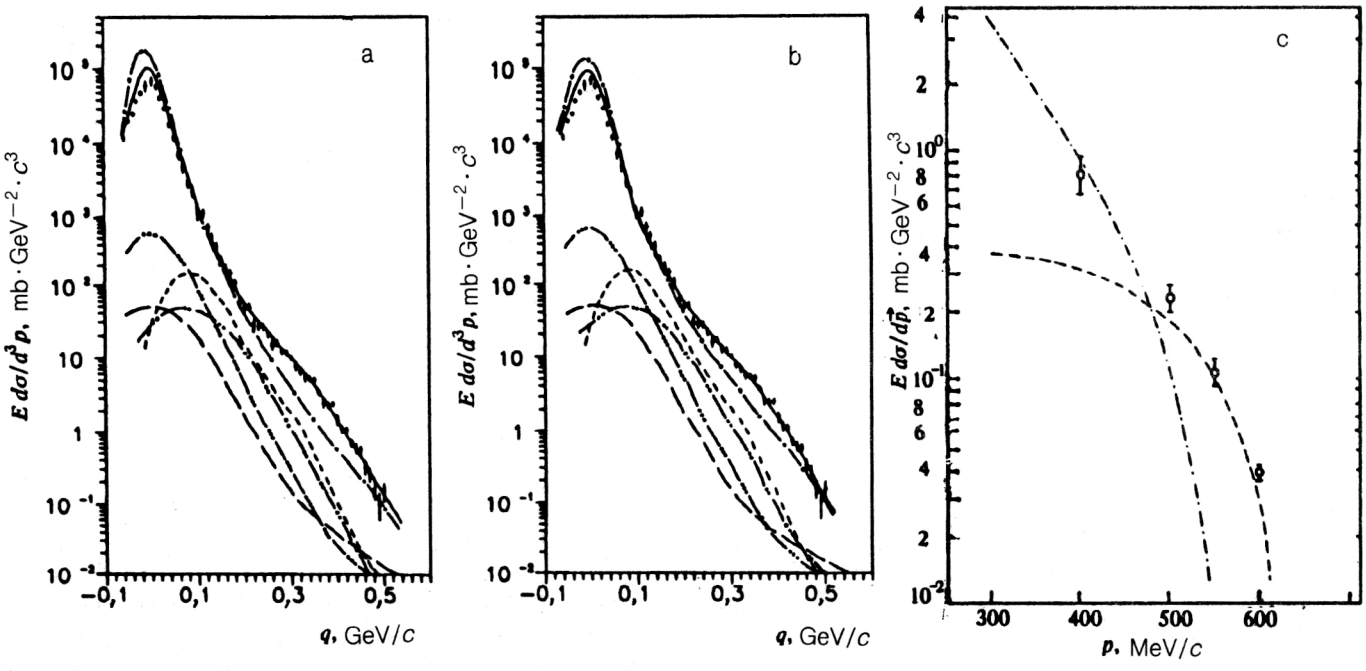

FIG. 6. Contributions of different mechanisms to the inclusive spectrum of protons from the reaction $dp \to pX$ at $p_d \approx 9$ GeV/c and proton emission angle $\theta_p \cong 0°$ calculated for a deuteron wave function of the type of Ref. 67 (a). The curves correspond to the following diagrams: the chain curve to Fig. 5a, the curve with three dots to Fig. 5b, the broken curve to the diagrams of Fig. 5c, the curve with two dots to Fig. 5d, the broken curve with long dashes to the diagrams of Fig. 5e, and the continuous curve to the sum of all diagrams of Fig. 5 with allowance for their interference. b) The same as in Fig. 6a, but for the Paris deuteron wave function.[68] c) Inclusive spectrum of protons produced in the $pd \to pX$ reaction at angle $\theta_p = 180°$ for initial momentum $p_0 \approx 9$ GeV/c. The chain curve gives the calculation in the impulse approximation (Figs. 5a and 5b). The broken curve gives the contribution of the non-nucleon degrees of freedom.[60] The experimental data are taken from Ref. 75.

contribution of such diagrams of the type of Fig. 5e was analyzed in Refs. 23, 48, and 49, admittedly with a nonrelativistic deuteron wave function. It was shown that this contribution is very sensitive to the form chosen for the deuteron wave function; the same conclusion was reached in our approach in Refs. 17, 35, and 36, in which the relativistic effects in the deuteron were taken into account by the method described above. As can be seen from Fig. 7, apart from the impulse approximation, the largest contribution to the proton spectrum is still made by diagrams with absorption of a virtual meson by a nucleon (Fig. 5c) and with πN rescattering (Fig. 5d), the contribution being approximately up to 60% for $0.2 < q < 0.4$ GeV/c.

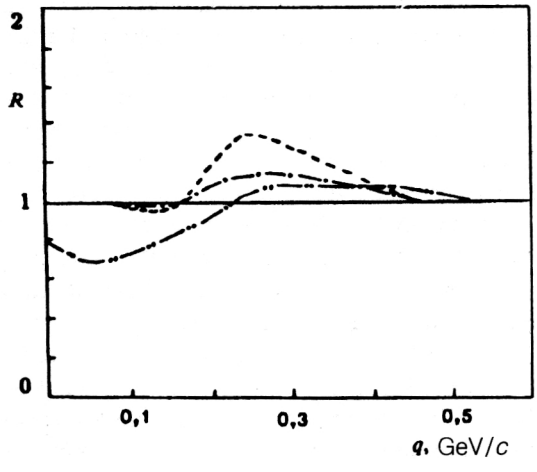

FIG. 7. Relative contributions of the two-step "mechanism" (Figs. 5c–5e) relative to the single-step mechanism (Figs. 5a and 5b) and their interference to the inclusive spectrum of protons in the deuteron-fragmentation reaction $dp \to pX$. The broken curve corresponds to the diagram of Fig. 5c, the chain curve to the diagram of Fig. 5d, and the broken curve with two dots to the diagram of Fig. 5e.

As the calculations of Refs. 17, 35, and 36 show, the polarization characteristics T_{20} and κ are more sensitive to allowance for the graphs of nonspectator type. The results of the calculation[35,36] of T_{20} and experimental data[41,50] are given in Fig. 8. It can be seen that allowance for all graphs of Fig. 5 gives a result that differs appreciably from the calculation in the framework of the spectator mechanism both in the region of the minimum of T_{20}, i.e., $0.2 < q < 0.4$ GeV/c, and at larger q. Of course, because of the large errors in the existing experimental data at $q > 0.4$ GeV/c it is not possible to say which sign T_{20} has in this region. Our calculation indicates a change in the sign of T_{20} at $q \cong 0.5$ GeV/c or $q \approx 0.54$ GeV/c, depending on the form of the deuteron wave function. Therefore, it would be extremely interesting to have more accurate experimental information on T_{20} at $q > 0.45$ GeV/c or $k > 0.7$ GeV/c, $x > 0.8$. This is particularly important for extracting new information on the relativistic structure of the deuteron and nonnucleon degrees of freedom, as will be discussed in detail below.

We now discuss the results of calculating the polarization transfer κ in $dp \to pX$ fragmentation; these are shown

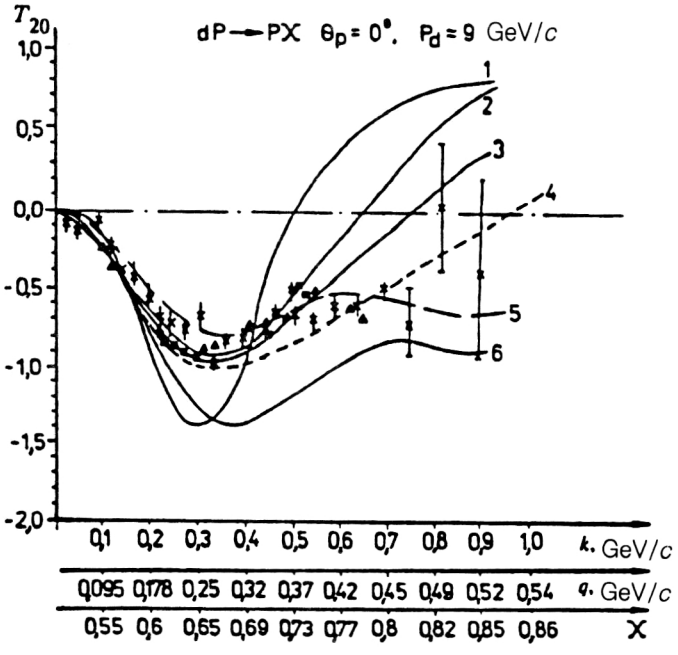

FIG. 8. Dependence of T_{20} on the momenta q and k and on the proton light-cone variable x. Curve *1* gives the contribution of the spectator mechanism (Fig. 5a), curve *2* is the contribution of the diagrams of Fig. 5a and 5c, and curve *3* is the contribution of all diagrams of Fig. 5. Curves *1*, *2*, and *3* correspond to calculations with a deuteron wave function of the type of Ref. 67. Curve *4* is the contribution of all diagrams of Fig. 5 but for the Paris deuteron wave function.[68] Curve *5* gives T_{20} with allowance for the composite $6q$ component calculated in Ref. 53, and curve *6* gives the result of the calculation of Ref. 16; the black triangles and squares are experimental data from Ref. 50, and the remaining data are from Refs. 3 and 41.

in Fig. 9 together with the available experimental data.[41,51,52] It can be seen that allowance for the two-step mechanism, i.e., the diagrams of Figs. 5c–5e, changes the values compared with the contribution of the simple spectator mechanism quite strongly in the interval $0.25 < q < 0.45$ GeV/c. The largest contribution to the change is made by the diagram of Fig. 5c with absorption of a virtual pion by a deuteron nucleon.

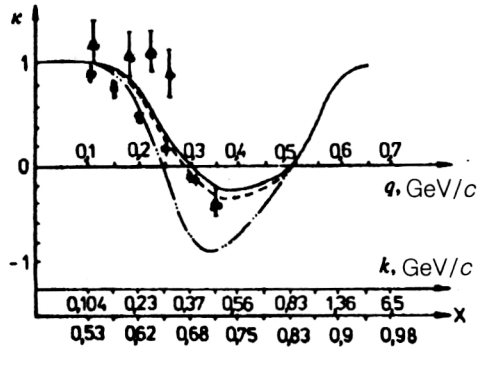

FIG. 9. Dependence of the polarization transfer κ on the momenta q and k and the variable x. The broken line with two dots gives the contribution of the spectator mechanism (Fig. 5a), the broken curve gives the contribution of the diagrams of Figs. 5a, 5b, and 5c, and the continuous curve gives the sum of all contributions of the diagrams of Fig. 5. All calculations were made using the Paris deuteron wave function. The black triangles are the experimental data from Refs. 3 and 41, and the black circles are from Ref. 52.

This can be explained by the fact that such absorption can be described by the πN interaction with pseudoscalar coupling, i.e., $\mathscr{L}_{\text{int}} = g(\bar{\Psi}\gamma_5\Psi)(\tau\varphi)$ (here, τ are isotopic matrices, and φ is the operator of the meson field), determining the spin-flip part of the total amplitude of the considered process. In other words, the terms proportional to $\vec{\sigma}\vec{p}'$ and $\vec{\sigma}\vec{k}_1$ in the expression for $\Gamma_N^{(2)}$ corresponding to the upper vertex of the diagram of Fig. 5c [see (15)] change the initial direction of the nucleon spin in the deuteron, and this influences the polarization $\vec{\mathscr{P}}'$ of the final protons or the polarization transfer κ. A similar effect is also obtained by considering the graph of Fig. 5d with rescattering of a pion on a deuteron nucleon, since the amplitude of elastic πN scattering also has a spin-flip part. Nucleon rescattering (see Fig. 5e) makes a small contribution to κ. This is explained by the fact that in our approach the spin dependence of the NN amplitudes is actually not taken into account; a justification for such an approximation for the investigated reaction is given in Ref. 36. This is due to the fact that the contribution of diagrams of the type of Fig. 5e when $q > 0.2$ GeV/c is greatest in the case of nucleon rescattering of Glauber type, i.e., with small transfers t in the lower and upper vertices of Fig. 5e, as calculations showed. But since the polarization effects in elastic NN scattering are small at small t, their spin dependence can be ignored.

We now consider the same observables ρ_{dN} and T_{20} but for the exclusive reaction $pd \to ppn$. At Jülich (Germany) there are plans for such an experiment in a proton beam with kinetic energy $T_0 \lesssim 2.5$ GeV and deuterium polarized and unpolarized targets.[73] It is planned to make the measurements under the following kinematic conditions: One proton is emitted forward and the other backward in the deuteron rest frame, or at angle θ_p near 180°, its momentum, energy, and emission angle being completely determined by the energy–momentum conservation laws for the complete $pd \to ppn$ reaction. We give predictions for the above observables in the exclusive reaction $pd \to ppn$ at $T_0 = 2.5$ GeV as a function of the momentum p_2 of the proton emitted at angle $\theta_p = 180°$ in the laboratory system. They are given in Fig. 10. It can be seen from Fig. 10a that the form of the spectrum $E_2 d\sigma/d^3p_2$ in the exclusive reaction is similar to the form of the inclusive spectrum in Fig. 6. However, at $T_0 = 2.5$ GeV there are quite significant effects of nucleon rescattering (the diagram of Fig. 5e) and also the final-state interaction, which decreases the cross section calculated in the impulse approximation (Figs. 5a and 5b) at $p_2 < 0.2$ GeV/c and increases it somewhat at $p_2 > 0.2$ GeV/c. The presence of an "excess" in the spectrum (see the continuous curve at $p_2 > 0.25$ GeV/c) is mainly due, as calculations[36] show, not to nucleon rescattering (Fig. 5e), but to the diagram of Fig. 5c with absorption of a virtual meson by a nucleon. This last fact is explained by the fact that the production of a pion in the $NN \to \pi NN$ reaction (see the lower vertex of Fig. 5c) at the initial energy $T_0 = 2.5$ GeV can also proceed through the

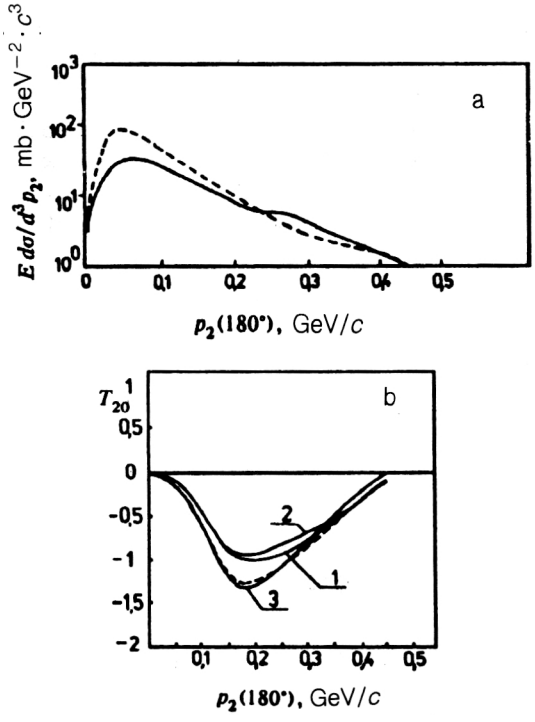

FIG. 10. Exclusive spectrum of a proton produced in the $pd \to ppn$ process at $T_p = 2.5$ GeV at angle $\theta_2 = 180°$ as function of its momentum p_2; the angle of the other proton is $\theta_1 = 0°$ (a). The broken curve is the contribution of the spectator graph (Fig. 4a); the continuous curve is the sum of all contributions of the diagrams of Fig. 4. b) The dependence of T_{20} on p_2 in the $pd \to ppn$ reaction under the same kinematic conditions as in Fig. 10a. Curves *1* and *2* are the sum of all contributions of the diagrams of Fig. 4 with the Paris deuteron wave function[68] and with a wave function of the type of Ref. 67; curve *3* gives the contribution of the pole diagrams of Fig. 4a for a deuteron wave function of the type of Ref. 67; the broken curve gives the same as curve *3* but with the Paris wave function.[68]

production of a Δ isobar in the intermediate state. With increasing initial energy T_0, this effect "dies out," and therefore, as can be seen from Fig. 6, such an "excess" does not arise in the spectrum of the inclusive reaction $pd \to pX$ at $T_0 \approx 4$ GeV.

Figure 10b gives the results of a calculation of T_{20} for the exclusive reaction $pd \to ppn$ at $T_{20} = 2.5$ GeV as a function of p_2. It can be seen that, as in the case of the inclusive reaction, a significant contribution to T_{20} in this process is made by the diagram of Fig. 5c with absorption of a virtual pion at $0.2 \lesssim p_2 \lesssim 0.4$ GeV/c. Further, as comparison of Fig. 7 and Fig. 10b shows, the energy dependence of T_{20} is very weak.

The physical consequences of the calculations of the observables in the inclusive and exclusive dp processes will be discussed in Sec. 5.

Note that the calculations of ρ_{dN} and T_{20} for the exclusive reaction $pd \to ppn$ were made in the framework of the approach presented above, based on Weinberg's diagrammatic technique. Formulas of the type (11)–(13) and (18) were used, but there was no integration in (11) or over the phase space in (18), since in the given case all the momenta and angles of the final particles are definite.

We now turn to analysis of the "hard" dN interaction (by this term, we mean the $dN \to pX$ process when the proton is emitted at a large angle $\theta_p \approx \pi/2$ in the deuteron rest frame) in the framework of the considered approach.

Hard *dN* scattering

We have considered the case of $dN \to pX$ fragmentation when the main contribution to the cross section of this process is made by the spectator diagram of Fig. 5a. We now analyze the case when the main contribution to this cross section will also be made by a pole but nonspectator diagram, i.e., the graph of Fig. 5b. The dN processes of this type include reactions in which one of the nucleons is emitted at a large angle near $\theta_p \approx 90°$ in the deuteron rest frame. The inclusive spectrum of protons produced in such kinematics in the $dN \to pX$ reaction can be calculated in the framework of our approach in accordance with Eq. (11) or (12) in the case of azimuthal symmetry of the final protons. There still remains the question of the contribution of the diagrams that make corrections to the diagram of Fig. 5b, i.e., the graphs of Figs. 5a and 5c–5e. In Refs. 53 and 54, calculations of ρ_{dN} for the inclusive process $dN \to pX$ when the protons are emitted at angle $\theta_p \approx 90°$ in the laboratory system were made. The calculations showed that the contribution of the spectator graph of Fig. 5a is in this case insignificant, and this is also true for the diagram with nucleon rescattering,[53] while the diagrams of Figs. 5c and 5d can make a significant contribution in a certain kinematic region, though admittedly less than in the case of dN fragmentation. Figure 11 gives the results of calculations of the inclusive proton spectra in the reaction for the kinematic conditions given above. The initial deuterons here have momentum $p_d = 8.9$ GeV/c. It can be seen from Fig. 11 that allowance for all graphs of Fig. 5 does not lead to a description of the available experimental data for $p > 5$ GeV/c or $x > 0.7$–0.8. As was noted above in the description of the inclusive spectrum of protons produced in dp stripping, there is also a discrepancy between the calculations and experiment at large x ($x > 0.8$). Therefore, in Ref. 60 an attempt was made to introduce a certain effective distribution of colorless three-quark clusters in a nucleus, in particular in the deuteron, taking into account non-nucleon degrees of freedom in it. In Fig. 11, curve *5* corresponds to allowance for such non-nucleon effects in the deuteron.[53] We shall discuss this problem in more detail in the following section.

Let us summarize what we have shown in this section, in which we have considered the mechanism of dp interaction at high energies in the framework of Weinberg's diagrammatic technique. From analysis of the proton spectra in fragmentation $dN \to pX$ and in the case when the protons are emitted at large angles in the deuteron rest frame it follows that the simplest impulse approximation by itself is not adequate to describe these spectra. As can be seen from Fig. 11, in the region $0.6 < x < 0.8$ other diagrams, those of Figs. 5c–5e, make a quite significant contribution. Moreover, we note that the individual graphs of Fig. 5 give different contributions to the proton spectra from deuteron fragmentation and from hard scattering, as can be seen from Figs. 6 and 11. For example, the diagrams of Fig. 5c with absorption of a virtual meson by a nucleon

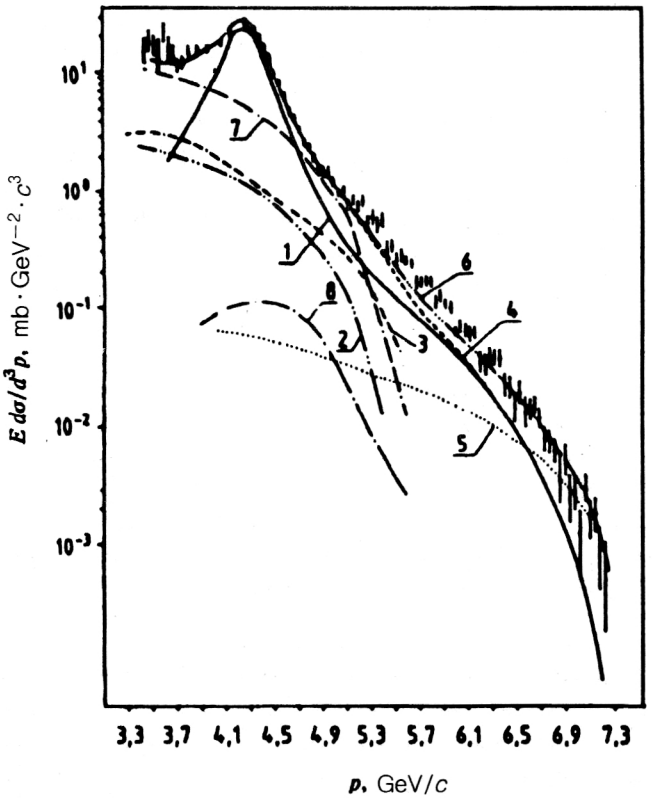

FIG. 11. Dependence of the inclusive invariant spectrum $E(d\sigma/d^3p)$ in the $dp\to pX$ reaction on the momentum of protons emitted at angle $\theta^*=90°$ in the NN center-of-mass system for $p_d\approx 9$ GeV/c. Curve *1* gives the contribution of the diagram of Fig. 5b corresponding to hard NN scattering, curve *2* gives the contribution of the diagram of Fig. 5c with a "soft" pion form factor (Ref. 53), curve *3* gives the contribution of the diagram of Fig. 5e, curve *4* gives the contribution of all diagrams of Figs. 5a–5e with a deuteron wave function $\Phi_{\text{n.r.}}$ of the type of Ref. 67, curve *5* gives the contribution of the non-nucleon degrees of freedom in the deuteron calculated in Ref. 53, and curve *6* gives the total contribution of the diagrams of Fig. 5 with allowance for the new deuteron function T_d of the form (25).[53,60] The experimental data are taken from Ref. 5.

make a larger contribution to the proton spectrum from deuteron fragmentation than in the case of "hard" dN scattering (cf. Figs. 6 and 11).

However, for $x>0.8$ the main contribution to the proton spectra in both cases is made by the impulse approximation, i.e., the graphs of Figs. 5a and 5b, and, as can be seen from Figs. 6 and 11, this approximation does not permit a description of the experimental data. This could be due to a possible manifestation of non-nucleon degrees of freedom in the deuteron.

4. NON-NUCLEON DEGREES OF FREEDOM IN THE DEUTERON

Deuteron-fragmentation processes at high energies are usually investigated with the aim of extracting new information on deuteron structure, especially at short distances or for large intradeuteron momenta k. However, as was shown in the previous section, the mechanism of the dN reaction with emission of high-energy protons cannot be reduced to the simple impulse approximation at not too large x, $x<0.8$. The spectator mechanism is dominant at small ($k<0.2$ GeV/c) and large k ($k>0.6$ GeV/c, $x>0.8$) in the dp stripping reactions, as can be seen from Fig. 6b. Therefore, only in these kinematic regions is the proton spectrum proportional to the square of the deuteron wave function, which determines the distribution of the nucleons in the deuteron:[35,34]

$$G_{N/d}=|\Psi(x,k_\perp)|^2/2(1-x).$$

Thus, at large x in the stripping process $dp\to pX$ the spectrum of cumulative protons at $x>0.8$ is largely determined by the spectator diagram of Fig. 5a, i.e., in this region

$$\rho_{dN}\simeq\frac{|\Psi(x,k_\perp)|^2}{2(1-x)}\sigma_{NN}^{\text{tot}}\equiv xG_{N/d}(x,k_\perp)\sigma_{NN}^{\text{tot}}; \qquad (24)$$

where the nucleon distribution function in the deuteron, $G_{N/d}(x,k_\perp)$, has been determined as in Refs. 5–7, 53, and 60.

However, as can be seen from Fig. 6c, the expression (24) for ρ_{dN} does not describe the proton spectrum in the stripping $dp\to pX$ at $x>0.85$. Therefore, using the connection (24) between ρ_{dN} and $G_{N/d}$, we can introduce the new function

$$T_d(x,k_\perp)=(1-\omega)G_{N/d}(x,k_\perp)+\omega\tilde{T}_d(x,k_\perp), \qquad (25)$$

which, when substituted in (24) or (11) in place of $G_{N/d}(x,k_\perp)$, would enable us to describe the experimental data presented in Figs. 6c and 11 near the kinematic limit. Here, ω is a parameter whose value can be determined from experimental data, as was done in Ref. 60.

It is well known that in the region of limiting fragmentation of nuclei and for $x'=p'/p_{\max}>1$ there was predicted in Ref. 55 and then experimentally found[1] a large contribution of cumulative, as they were subsequently called,[1,8,56] particles (here, p' is the momentum of a hadron produced in hA collisions, and $p_{\max}$ is the maximum momentum of the same hadron but produced in hN collisions on the free nucleon).

As was shown in Refs. 2 and 57, the ordinary Fermi motion of nucleons in a nucleus cannot explain the rather large cross section for the production of cumulative particles at large x', and one must introduce the hypothesis that there are either many-quark fluctons in a nucleus[2,4,58] or short-range few-nucleon correlations.[18,30] The effective nucleon distribution in the nucleus, T_A, can be represented in these cases in the form[4,60]

$$T_A(\alpha)=\sum_{k=1}^{A}P_k^A T_k(\alpha), \qquad (26)$$

where P_k^A is the probability of a $3k$-quark (or k-nucleon) correlation, and $T_k(\alpha)$ is the effective distribution of the "nucleons" or $3q$-colorless clusters in such a formation.

We now attempt to determine the analytic form of $T_A(\alpha)$ at least at large α ($\alpha>1$); at small α ($\alpha<1$), $T_A(\alpha)$ is, as was noted above, the usual Fermi distribution $G_{N/A}$ of nucleons in the nucleus. For this, we must, in accordance with (26), determine the form of $T_k(\alpha)$.

The quark distribution in the nucleus, $q_A(x')$, can be related to the quark distribution in the nucleon as follows:[60]

$$q_A(x')=\int_{x'}^{A} T_A(\alpha)q_N(x'/\alpha)d\alpha. \tag{27}$$

For the distribution of the quarks in the $3k$-quark colorless system we obtain from this

$$q_k(x')=\int_{x'}^{k} T_k(\alpha)q_N(x'/\alpha)d\alpha. \tag{28}$$

We now determine the form of $q_k(x')$ at large x' ($x'>1$) from the Regge behavior of this quark structure function as $x'\to k$. This behavior is determined by the probability that one of the quarks of the k-cluster is fast, i.e., carries almost all the cluster momentum, while the remainder are slow (wee quarks). Calculating this probability in the framework of the quark–gluon string model,[59] we can obtain the following expression for the quark distribution:[60]

$$q_k(x')\sim x_k^{-\alpha_R(0)}(1-x_k)^{2[1-\bar{\alpha}_B(0)](k-1)+b_N},$$

$$b_N=\alpha_R(0)-2\bar{\alpha}_N(0),$$

where $x_k=x'/k$; $\bar{\alpha}_N(0)=-0.5$, $\alpha_R(0)=0.5$, $\bar{\alpha}_B(0)=-0.5$–0.0; $\alpha_R(0)$, $\alpha_N(0)$, $\bar{\alpha}_B(0)$ are the intercepts of the boson, (ρ,f,A_2,ω), and averaged nucleon and baryon, (N,Δ), Regge trajectories. The term $b_N=\alpha_R(0)-2\bar{\alpha}_N(0)\approx 3/2$ in the exponent of $q_k(x')$ corresponds to the distribution of the valence quarks in the nucleon,[59] and the additional factor $(1-x_k)^{2[1-\bar{\alpha}_B(0)](k-1)}$ is associated with the probability of slowing down of $k-1$ nucleons (quarks and diquarks).[59] Substituting $q_k(x')$ in (26), at large α we now have approximately

$$T_k(\alpha)=C_k\alpha^{A_k}(k-\alpha)^{B_k}, \tag{29}$$

where $B_k=2[1-\bar{\alpha}_B(0)](k-1)-1$. The values of A_k and C_k are determined from the normalization conditions

$$\int_0^A T_k(\alpha)d\alpha=1; \quad \int_0^A \alpha T_k(\alpha)d\alpha=1-\Delta_k,$$

which follow from the normalization condition for $T_A(\alpha)$ given above. Here, Δ_k determine the momentum of the so-called collective sea in a k-flucton,[60,61] i.e., the distribution of the sea quarks in it. This distribution differs strongly from the corresponding distribution of the sea quarks in a free nucleon.

We now turn to the analysis of the deuteron structure function and the function $T_d(\alpha)$. In accordance with (26),

$$T_d(\alpha)=P_1^dT_1(\alpha)+P_2^dT_2(\alpha). \tag{30}$$

Comparing the expressions (25) and (30), we obtain

$$P_1^d=1-\omega; \quad P_2^d=\omega; \quad T_1=G_{N/d}; \quad T_2=\tilde{T}_d;$$

i.e., $P_1^d=1-P_2^d$.

Here, P_1^d is the probability that the deuteron consists of ordinary nucleons, and P_2^d is the probability for existence in the deuteron of non-nucleon states.[60]

The functional form of $T_2(\alpha)$ is now determined by the expression (29) with $k=2$. We determine P_2^d, Δ_2, $\bar{\alpha}_B^{(0)}$ as parameters.

Thus, in accordance with (24), the invariant spectrum of protons produced in deuteron stripping $dp\to pX$ at large α ($\alpha>2\cdot 0.85$, i.e., $\alpha>1.7$) can be defined as

$$\rho_{dN}(\alpha)\sim\alpha T_d(\alpha)\sigma_{NN}^{\text{tot}}. \tag{31}$$

From the experimental data on ρ_{dN} the parameters of the function $T_d(\alpha)$ were determined, and the data on deuteron stripping $dp\to pX$ (Refs. 3, 41, 62, and 63) were fitted.[60] The scaling variable used here was x_S, the so-called Stavinskiĭ variable,[8] which takes into account the fact that the energy of the initial particle is not infinite but has a certain finite value. In accordance with (24),

$$T_1(x_S)=G_{N/d}(x_S/2)=\frac{|\Psi(x_S/2)|^2}{2(1-x_S/2)}. \tag{32}$$

Note that the experimental data on $Ed\sigma/d^3p$ have different normalization coefficients. Therefore, they determine only the shape of the inclusive proton spectrum. Since $T_d(\alpha)$ determines only the shape of the momentum spectrum, each group of data is fitted in accordance with Eq. (31) with its own normalization coefficient. These experimental data (corrected to the corresponding coefficients, i.e., agreeing in magnitude at $x_S/2=0.5$) and the curves obtained by fitting are shown in Fig. 12. The values of the parameters were found to be

$$\bar{\alpha}_B(0)=-0.05; \quad \Delta_2=0.34; \quad P_2^d=3.6\%.$$

Note that the fitting was done only for the high-energy part of the spectrum [i.e., for $x_S/2>0.85$, when the relation (31) is valid], which is described mainly by $T_2(x_S)$. In other words, in the complete $T_d(x_S)$ determined by (30) only its part $T_2(x_S)$ was fitted, the aim being to describe only the spectrum at $x_S/2>0.85$, since for $x_S/2<0.85$ the spectrum is described not only by the spectator mechanism but also by the diagrams considered in the previous section. Therefore, the discrepancy between the data in Fig. 12 and the continuous curve calculated in the spectator mechanism in the region $0.7<x_S/2<0.85$ is explained, as was shown in Secs. 1 and 2, by diagrams that are not taken into account here.

We now consider the nuclear structure function F_A. In the classical potential picture of a nucleus, any structure function can be expressed in terms of the distribution T_A of the nucleons in the nucleus and the nucleon structure function F_N. In our case, T_A is, as we have noted above, a certain effective distribution of colorless $3q$ clusters ("nucleons"). Such a connection between F_A and F_N can be expressed in the form of a so-called Mellin convolution:[60,61]

$$F_A(x_B,Q^2)=\int_{x_B}^{A} T_A(\alpha)F_N\left(\frac{x_B}{\alpha},Q^2\right)d\alpha. \tag{33}$$

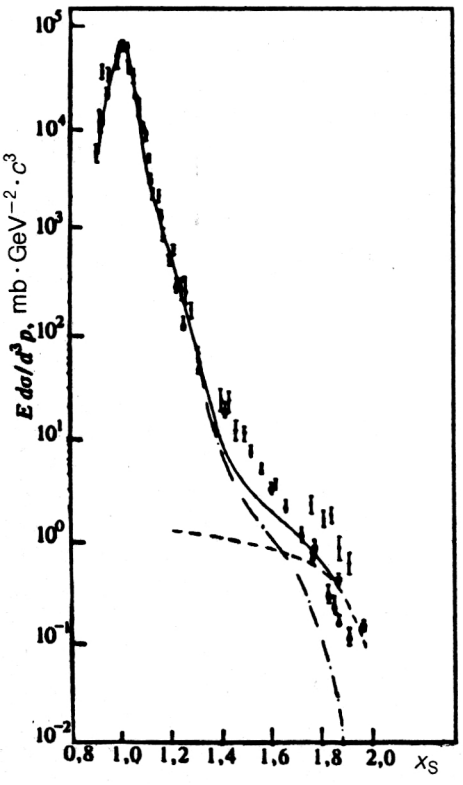

FIG. 12. Inclusive proton spectrum in the $pd \to pX$ reaction when the protons are emitted at angle $\theta_p = 180°$ in the deuteron rest frame. The chain curve gives the contribution of the spectator mechanism (Fig. 5a), the continuous curve gives the contribution of the diagram of Fig. 5a but with the function T_d (25), and the broken curve gives the contribution of only the non-nucleon component in the deuteron. For the experimental data, see the references in Ref. 60.

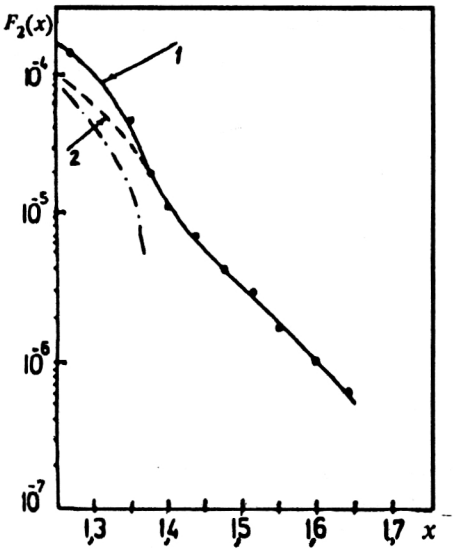

FIG. 13. The structure function $F_{2d}(x)$. The chain curve gives the calculation with the Paris deuteron wave function[68] and $P_2 = 0$. The remaining curves are the result of the calculation of $F_{2d}(x)$ with allowance for the non-nucleon component in the deuteron, $P_2^d \approx 3.6\%$ (Ref. 60): curve *1* with a parametrization of F_{2N} of the type of Ref. 62 for $Q^2 < 4$ $(\text{GeV}/c)^2$, and curve *2* with a parametrization of F_{2N} of the type of Ref. 63 for $Q^2 > 4$ $(\text{GeV}/c)^2$. The continuous curve is the result of combining curves *1* and *2*, and the experimental points are SLAC data.[66]

Using the calculated effective nucleon distribution in the deuteron, we now test the relation (33) for the deuteron structure function F_{2d}. We shall use SLAC data[66] in the region of the Bjorken variable $x_B \gtrsim 1$ at $Q^2 = 2$–8 $(\text{GeV}/c)^2$. The results of such an investigation are shown in Fig. 13. The first two experimental points in the figure, at $x_B = 1.27$ and $x_B = 1.35$, correspond to $Q^2 < 4$ $(\text{GeV}/c)^2$, and the remainder to $Q^2 > 4$ $(\text{GeV}/c)^2$. Therefore, to calculate F_{2d} from (33) we used for F_{2N} the parametrization of Ref. 62, which is valid for $Q^2 < 4$ $(\text{GeV}/c)^2$, $x < 1.4$, and the parametrization of Ref. 63 for $Q^2 > 4$ $(\text{GeV}/c)^2$, $x > 1.4$ (continuous curve in Fig. 13). The chain curve corresponds to allowance for only the nucleon component in the deuteron wave function, i.e., $P_2^d = 0$ (30), and Ψ was taken to be the Paris deuteron wave function.[68] It can be seen that in the region $x_B > 1$ the agreement is quite good within the experimental errors, and from this we may conclude that the function T_d is close to the effective distribution of the nucleons in the deuteron.

We now consider the change in the result if we substitute in place of $G_{N/d}$ introduced in (24) the function T_d in order to calculate the proton spectrum in the $dp \to pX$ reaction when the protons are scattered at large angle in the NN center-of-mass system at large x. The internal transverse motion of the quarks will be ignored in this calculation. In Fig. 11, curve *5* shows the contribution of $T_2(x')$ to the inclusive momentum distribution of the protons. It can be seen that the agreement between the calculations in Fig. 11 and the experimental data is greatly improved for $p > 6.5$ GeV/c or $x_S/2 > 0.8$. Thus, the function T_d found from the deuteron-stripping process has made it possible to describe the data on the production of protons in the process $dp \to pX$ at large x when they are emitted at large angles in the center-of-mass system of the two nucleons.

We have considered only one of the possible approaches to the investigation of the deuteron in the analysis of deuteron fragmentation; it was proposed earlier in Refs. 60 and 61. In reality, there are several other approaches to the investigation of non-nucleon structure of the deuteron. Numerous reviews have been published on this subject (Refs. 2, 4, 58, and 8), and therefore we shall not dwell on this in detail. Here, we merely mention a problem that can be encountered in the analysis of six-quark states in the deuteron and is associated with relativistic effects in it. In some model approaches to the investigation of the deuteron quark structure, the analysis is made in the framework of a nonrelativistic approximation,[14] i.e., the relativistic effects in the deuteron are completely ignored. The importance of taking into account relativistic effects in the deuteron can be demonstrated for the example of the so-called minimum relativization of the deuteron wave function.[66,67] At the end of the fifties, Shapiro showed[66] that in the general relativistic case the transformation properties of the wave function of a free spinless particle are different from the nonrelativistic case. In other words, the wave function in the coordinate space is related to the wave function in the momentum space as follows:[66]

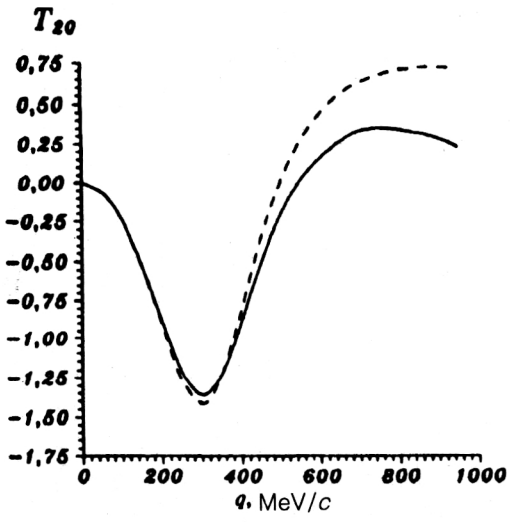

FIG. 14. Dependence of T_{20} on the momentum q of the spectator nucleon in the stripping reaction $dp \to pX$ at $p_d \approx 9$ GeV/c. The continuous curve gives the result of a calculation in the framework of the spectator mechanism (Fig. 5a) with relativized Paris deuteron wave function.[68] The broken curve gives the result with a nonrelativized deuteron wave function of the same type.[68]

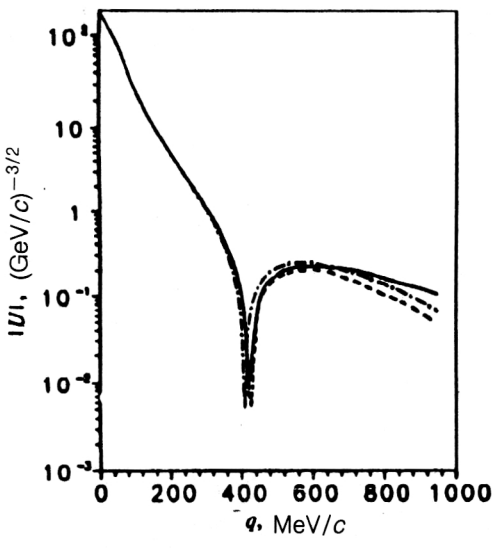

FIG. 15. Momentum distribution of the S wave of the Paris deuteron wave function. The broken curve gives the calculation with the nonrelativistic deuteron wave function, and the chain curve corresponds to the S wave of the Paris deuteron wave function but with allowance for the $6q$ component[76] in the framework of the hybrid quark model.[14]

$$\tilde{\Psi}(p)=\frac{1}{(2\pi)^{3/2}}\int \xi(p,r)\Psi(r)d^3r, \tag{34}$$

$$\xi(p,r)=\left(\frac{\omega_p-pr_0}{m}\right)^{1-im|r|}, \tag{35}$$

where $r_0=r/|r|$, $\omega_p=(p^2+m^2)^{1/2}$.

The wave function $\tilde{\Psi}(p)$, which is related to $\Psi(r)$ by the expressions (34) and (35), has the following properties: 1) It transforms in accordance with an irreducible representation of the Lorentz group; 2) it has an invariant normalization (Ref. 70); 3) it becomes the ordinary Fourier transform in the nonrelativistic case, i.e., in the limit $r \to \infty$ the function $\xi(p,r)$ goes over into $\exp(i\vec{p}\vec{r})$.

We now consider what happens if, in calculating observable quantities, we replace the nonrelativistic Fourier transform of the wave function by transformations of the form (34), considering, for example, the behavior of T_{20} in $dp \to pX$ stripping and in the deuteron wave function itself.

Figure 14 demonstrates the sensitivity of T_{20} to the different ways of transforming $\Psi(r)$ (Fourier and Shapiro). The calculations of T_{20} were made in the framework of the spectator mechanism. It can be seen from the figure that the effect of "minimum relativization" gives a shift in the behavior of T_{20} to the region of large q, $q \gtrsim 0.4$ GeV/c. Figure 15 shows the momentum distribution of the S wave of the Paris deuteron wave function[68] (broken curve). The chain curve in Fig. 15 corresponds to the behavior of the S wave calculated in the framework of the hybrid quark model[14,76] with the Paris potential[68] with the weight of the six-quark component in the deuteron taken to be 2.5%.[76] The continuous curve in Fig. 15 corresponds to the momentum distribution of the S wave of the deuteron wave function, $\tilde{u}(p)$, obtained by means of the Fourier transformation (34) from the Paris deuteron wave function in the r space. Thus, it can be seen from this figure that the "minimum relativization" of the deuteron wave function imitates the behavior of the deuteron wave function in the hybrid quark model[14] with a nonrelativistic potential, particularly in the region $q \approx 0.4$ GeV/c. Therefore, it is clear that only for a correct description of the internal structure of a relativistic system, in particular the deuteron, can one understand the actual contribution of the six-quark configuration to the deuteron wave function.

Figure 16 gives the momentum distributions, nonrelativistic, $\Psi(q)$, and relativistic, $\tilde{\Psi}(q)$, of different deuteron wave functions (Paris and Bonn[72]). It can be seen that the effect of "minimum relativization" can be quite large for $q > 0.4$ GeV/c. It can also be seen from Fig. 16 that the Shapiro transformation leads to enhancement of the large-momentum component of the deuteron wave function. This was also pointed out in Ref. 73.

Of course, the Shapiro transformation of $\Psi(r)$ by itself cannot be the solution to the problem of relativization of the wave function of a bound state. However, the demonstrated sensitivity of the different physical quantities to different transformations of $\Psi(r)$ (see Figs. 14–16) shows the exceptional importance of taking into account relativistic effects in the deuteron, especially at $q > 0.4$ GeV/c or small r ($r < 0.5$ fm).

5. PROSPECTS FOR THEORETICAL AND EXPERIMENTAL INVESTIGATION OF DEUTERON STRUCTURE

We first summarize what we have presented in the previous sections.

1. It is quite incorrect to use a nonrelativistic deuteron wave function in the analysis of dN processes like fragmen-

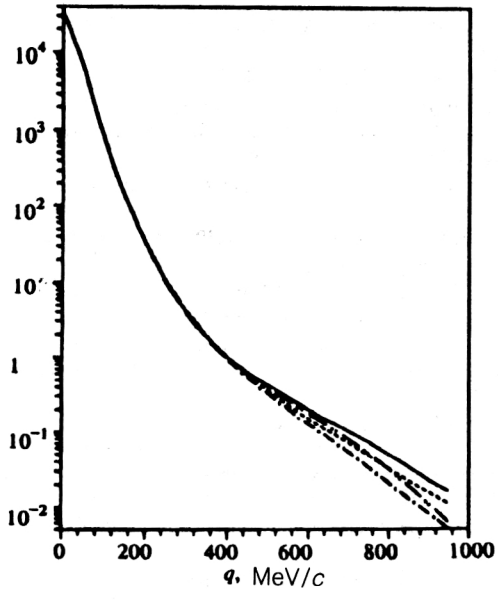

FIG. 16. Momentum distribution of nucleons in the deuteron, i.e., $|\Psi|^2$ in the units GeV^{-3}. The broken and chain curves give the results of calculations with nonrelativistic deuteron wave functions—Paris and Bonn, respectively. The continuous curve and the broken curve with two dots give the calculation with the same wave functions but relativized accordingly.

tation or hard NN interactions. Relativistic effects are particularly important in the kinematic region corresponding to short intradeuteron distances r.

2. At the present time, the state of the theory is such that a unique procedure for taking into account relativistic effects in the deuteron has not yet been found. Extreme sensitivity to the different methods of relativizing the deuteron wave function is found for the polarization characteristics in inclusive and exclusive $d \to N$ reactions, especially at large intradeuteron momenta. The momentum spectra of the protons produced in such processes are less sensitive to the different methods.

3. Nonrelativistic quark models using nonrelativistic potentials, as, for example, in the hybrid model, can distort the information on the quark structure of the deuteron, particularly at short distances, $r < 0.5$ fm, owing to the neglect of the relativistic effects in the deuteron, which are important in this region. This is illustrated by the results of the calculations presented in Figs. 12–14 in Sec. 4.

4. Analysis of the mechanism of $d \to N$ reactions at high energies shows that it is quite inadequate to restrict the treatment to just the pole approximation. The contribution of the nonpole diagrams—nucleon or meson rescattering in the intermediate state, and diagrams with absorption of virtual mesons by a nucleon—may be comparable with the contribution of the pole diagrams, especially for $0.6 < x < 0.8$.

5. All the observable quantities in the considered $d \to N$ processes, particularly polarization phenomena, are sensitive to the reaction mechanism at $x < 0.8$.

6. At $x > 0.8$, analysis of $d \to N$ processes, stripping, and "hard" dN scattering shows that the contributions of the nonpole diagrams gradually decrease, and the pole diagrams or the diagrams of single NN interaction make the main contribution, at least to the momentum spectra of the protons. However, the latter diagrams do not describe the existing experimental data at $x > 0.8$.

7. Allowance for non-nucleon degrees of freedom in the deuteron may make it possible to describe the experimental data on the proton spectra at $x > 0.8$. However, this cannot be a direct and unambiguous proof of their existence, since there are other possible explanations of the large-momentum part of the proton spectra.[71,72]

8. At the same time, these non-nucleon degrees of freedom in the deuteron are extremely important for describing the spectra of cumulative mesons already when $x' > 1$,[60] i.e., $x > 0.5$. The ordinary distribution of nucleons in the deuteron, for example, of the type of Refs. 67 and 68, does not permit description of the inclusive spectra of mesons produced in pd interactions in the cumulative region, i.e., $x' > 1$ ($x > 0.5$), as is clearly shown in Refs. 2 and 57.

From all that has been said above, it may be concluded that the most favorable kinematic region for investigating deuteron structure in dN processes is the region of large momenta of the scattered protons ($x > 0.7$–0.8) or of the produced hadrons ($x' = 2x > 1$). At the present time, there is, unfortunately, little experimental information on the spectra of the cumulative protons produced in the $dp \to pX$ reaction at $x > 0.7$–0.8. Therefore, it is very desirable to have such data, moreover not only at $\theta_p \cong 180°$ in the deuteron rest frame[72] but also at other angles. This is needed, on the one hand, to allow extraction of nontrivial information on the deuteron structure at short intradeuteron distances from these data and, on the other, to test the predictions of the different theoretical models.

Study of polarization phenomena in dp interactions, both inelastic and elastic, is particularly interesting, since, as was shown in Sec. 3 and in Refs. 17, 35, and 36, the polarization characteristics are extremely sensitive to the deuteron structure, especially at large intradeuteron momenta or short internucleon distances. Experimental information on such phenomena in reactions, for example, in deuteron stripping, is rather sparse for $k > 0.7$–0.8 GeV/c. There are only experimental data[41] on T_{20} in this kinematic region, but with large errors. If the most complete experiment proposed in Ref. 63 were performed, i.e., measurements were made of the momentum spectrum of the protons, T_{20}, and other polarization characteristics, for example, the polarization transfer $\kappa = \vec{\mathcal{P}}'/\vec{\mathcal{P}}$, the polarization correlations, etc., especially in the region of large k, it would be possible to extract new information on the deuteron structure at short internucleon distances. For this purpose, measurements of observables in exclusive experiments seem to us rather interesting. It will be desirable to have high energies of the initial particles in order to investigate the dp processes, for example, deuteron fragmentation at large intradeuteron momenta or "hard" dp scattering at large transfers t.

As follows from the above, investigation of dp processes at, for example, energies $T_d \lesssim 4$–5 GeV will give additional information about the reaction mechanism rather than about its structure. This can be explained by

the fact that at such initial energies it is impossible to penetrate to short intradeuteron distances, for example, $r_N < 0.5$ fm. In this connection, we briefly consider one of the projects for new experiments at Jülich, where it is intended to measure observable quantities in the $pd \to ppn$ reaction at $T_p \lesssim 2.5$ GeV when one of the detected protons is emitted forward and the other backward. As can be seen from Fig. 10, the momentum spectrum of the protons emitted backward in this reaction and the deuteron tensor analyzing power T_{20} are qualitatively similar to the same observable quantities but in the exclusive $dp \to pX$ reaction. Therefore, the conclusions drawn for the inclusive dp process can also be applied for the exclusive reaction. This, in its turn, means that it is also desirable to study the exclusive process $pd \to ppn$ experimentally at high initial energies, especially at energies for which it is possible to measure the spectrum of the protons emitted backward, at $x > 0.7$–0.8.

On the other hand, if we have experimental information on the various observable quantities in the $pd \to ppn$ process at $T_p \lesssim 2.5$ GeV in the experiment mentioned above, this will be helpful for studying the reaction mechanism and for obtaining nontrivial new information on off-mass-shell effects of the nucleons in the deuteron. The fact is that in the kinematic region in which one proton is emitted backward and the other forward there is strong manifestation of the off-shell effects, i.e., $k_N^2 \neq m^2$, where k_N is the 4-momentum of a nucleon in the deuteron, particularly at large momenta of the detected proton.

Besides the investigation of the cumulative processes of production of nucleons or other hadrons in pd reactions, as has frequently been reported (Refs. 1–4, 41, and 63), it is worth studying below-threshold production of particles, for example, K mesons, η mesons, antiprotons, etc. The reason for this is that by studying the production of such hadrons beyond the threshold for their production in proton collisions on the free nucleon one can obtain nontrivial information on the deuteron structure, particularly at large intradeuteron momenta.

In conclusion, I should like to emphasize once more that the development of the relativistic theory of deuteron structure appears very interesting and promising and is particularly important in the region of short intradeuteron distances.

[1] A. M. Baldin, Fiz. Elem. Chastits At. Yadra **8**, 429 (1977) [Sov. J. Part. Nucl. **8**, 175 (1977)].
[2] V. K. Luk'yanov and A. I. Titov, Fiz. Elem. Chastits At. Yadra **10**, 815 (1979) [Sov. J. Part. Nucl. **10**, 321 (1979)].
[3] V. G. Ableev *et al.*, Pis'ma Zh. Eksp. Teor. Fiz. **37**, 196 (1983); **47**, 613 (1988) [JETP Lett. **37**, 233 (1983); **47**, 279 (1988)].
[4] A. V. Efremov, Fiz. Elem. Chastits At. Yadra **13**, 613 (1982) [Sov. J. Part. Nucl. **13**, 254 (1982)].
[5] L. S. Azhgireĭ *et al.*, Yad. Fiz. **46**, 1353 (1987) [Sov. J. Nucl. Phys. **46**, 796 (1987)].
[6] I. A. Schmidt and R. Blankenbecler, Phys. Rev. D **15**, 3321 (1977).
[7] Wong Cheuk-Yin and R. Blankenbecler, Phys. Rev. C **22**, 2433 (1980).
[8] V. S. Stavinskiĭ, Fiz. Elem. Chastits At. Yadra **10**, 949 (1979) [Sov. J. Part. Nucl. **10**, 373 (1979)].
[9] R. G. Arnold, C. F. Carlson, and P. Gross, Phys. Rev. C **23**, 363 (1981).
[10] M. P. Rekalo, in *Proc. of the Third International Symposium: Pion–Nucleon and Nucleon–Nucleon Interactions*, Vol. 2 [in Russian] (Leningrad, 1989), p. 200.
[11] J. J. Aubert *et al.*, Phys. Lett. **123B**, 275 (1983).
[12] R. G. Arnold *et al.*, Phys. Rev. Lett. **52**, 727 (1984).
[13] A. P. Kobushkin and V. P. Shelest, Fiz. Elem. Chastits At. Yadra **14**, 1146 (1983) [Sov. J. Part. Nucl. **14**, 483 (1983)].
[14] V. G. Neudachin, I. T. Obuchovsky, V. I. Kukulin *et al.*, Phys. Rev. C **11**, 128 (1975).
[15] V. A. Karmanov, Fiz. Elem. Chastits At. Yadra **19**, 525 (1988) [Sov. J. Part. Nucl. **19**, 228 (1988)].
[16] M. A. Braun and M. V. Tokarev, Fiz. Elem. Chastits At. Yadra **22**, 1237 (1991) [Sov. J. Part. Nucl. **22**, 601 (1991)].
[17] M. G. Dolidze and G. I. Lykasov, in *Proc. of the 25th Winter School of the Leningrad Institute of Nuclear Physics*, Vol. 3 [in Russian] (Leningrad, 1990), p. 187.
[18] L. L. Frankfurt and M. I. Strikman, Phys. Rep. **5**, 215 (1981).
[19] A. P. Kobushkin and L. J. Vizireva, J. Phys. G **6**, 893 (1982).
[20] N. S. Amelin, V. V. Glagolev, and G. I. Lykasov, Fiz. Elem. Chastits At. Yadra **13**, 130 (1982) [Sov. J. Part. Nucl. **13**, 55 (1982)].
[21] V. B. Kopeliovich and V. V. Radomanov, Preprint R2-671 [in Russian], JINR, Dubna (1978).
[22] M. A. Braun and V. V. Vechernin, Yad. Fiz. **28**, 1466 (1978) [Sov. J. Nucl. Phys. **28**, 753 (1988)].
[23] L. G. Dakhno and V. A. Nikonov, Yad. Fiz. **50**, 1757 (1989) [Sov. J. Nucl. Phys. **50**, 1091 (1989)].
[24] F. Gross, Phys. Rev. **100**, 223 (1974).
[25] V. R. Garsevanishvili, in *Thirteenth Winter School of Theoretical Physics in Karpacz*, Vol. 1 (1976), p. 313.
[26] V. G. Kadyshevskiĭ, Zh. Eksp. Teor. Fiz. **46**, 654, 872 (1964) [Sov. Phys. JETP **19**, 443, 597 (1964)]; Nucl. Phys, **B6**, 125 (1968).
[27] S. Weinberg, Phys. Rev. **150**, 1313 (1966).
[28] S. J. Brodsky *et al.*, Phys. Rev. D **8**, 4574 (1973).
[29] J. B. Kogut and D. E. Soper, Phys. Rev. D **1**, 2901 (1970).
[30] M. I. Strikman and L. L. Frankfurt, Fiz. Elem. Chastits At. Yadra **11**, 571 (1980) [Sov. J. Part. Nucl. **11**, 221 (1980)].
[31] J. A. Tjon and G. Rupp, Phys. Rev. C **41**, 472 (1990).
[32] V. V. Anisovich and A. V. Sarantsev, in *Proc. of the 25th Winter School of the Leningrad Institute of Nuclear Physics*, Vol. 1 [in Russian] (Leningrad, 1990), p. 49.
[33] I. L. Grach and L. A. Kondratyuk, Yad. Fiz. **39**, 316 (1984) [Sov. J. Nucl. Phys. **39**, 198 (1984)].
[34] F. M. Lev, Fiz. Elem. Chastits At. Yadra **21**, 1251 (1990) [Sov. J. Part. Nucl. **21**, 534 (1990)].
[35] M. G. Dolidze and G. I. Lykasov, Z. Phys. A **336**, 339 (1990).
[36] M. G. Dolidze and G. I. Lykasov, in *Proc. of the 10th Intern. Seminar on High Energy Physics Problems*, Vol. 11 (JINR, Dubna, 1990), p. 336; Yu. L. Dorodnych and G. I. Lykasov, Preprint No. 781/92, Institute of Nuclear Physics, Moscow (1992).
[37] H. Grassler *et al.*, Nucl. Phys. **B132**, 1 (1978).
[38] T. Akesson *et al.*, Nucl. Phys. **B203**, 27 (1982).
[39] M. G. Golidze *et al.*, Z. Phys. A **325**, 391 (1986).
[40] N. S. Amelin and G. I. Lykasov, Yad. Fiz. **28**, 1258 (1978) [Sov. J. Nucl. Phys. **28**, 648 (1978)].
[41] V. G. Ableev *et al.*, in *Proc. of the Seventh Intern. Conf. on Polarization Phenomena in Nuclear Physics*, Vol. 1 (Paris, 1990), p. 40F.
[42] V. S. Barashenkov and N. V. Slavin, Fiz. Elem. Chastits At. Yadra **15**, 997 (1984) [Sov. J. Part. Nucl. **15**, 446 (1984)].
[43] L. A. Ponomarev, Fiz. Elem. Chastits At. Yadra **7**, 186 (1976) [Sov. J. Part. Nucl. **7**, 70 (1976)].
[44] Yu. L. Dorodnych, V. G. Neudachin, N. P. Yudin, and I. T. Obuchovsky, Phys. Rev. C **43**, 2499 (1991).
[45] S. S. Vasan, Phys. Rev. D **8**, 4092 (1973).
[46] L. I. Lapidus, Fiz. Elem. Chastits At. Yadra **15**, 493 (1984) [Sov. J. Part. Nucl. **15**, 223 (1984)].
[47] D. V. Bugg and C. Wilkin, Nucl. Phys. **A467**, 565 (1987); Phys. Lett. **152B**, 37 (1985).
[48] C. F. Perdrisat and V. Punjabi, Phys. Rev. C **42**, 1899 (1989).
[49] L. G. Dachno and V. A. Nikonkov, Nucl. Phys. **A491**, 6521 (1989).
[50] C. F. Perdrisat *et al.*, Phys. Rev. Lett. **59**, 2840 (1987).
[51] A. V. Zarubin *et al.*, in *Proc. of the Dubna Workshop on Problems of Deuteron Structure at High Energies*, E2-92-25, JINR, Dubna (1991), p. 214.
[52] C. F. Perdrisat *et al.*, in *Proc. of the Dubna Workshop on Problems of*

Deuteron Structure at High Energies, E2-92-25, JINR, Dubna (1992), p. 179.
[53] M. G. Dolidze and G. I. Lykasov, Z. Phys. A **335**, 95 (1990).
[54] L. S. Azhgirey *et al.*, Nucl. Phys. **A528**, 621 (1991).
[55] A. M. Baldin, Kratk. Soobshch. Fiz. **1**, 35 (1971).
[56] A. M. Baldin, in *Proc. of the Rochester Meeting* (APS, New York, 1971), p. 131.
[57] S. B. Gerasimov and N. Giordenescu, Communication R2-7687 [in Russian], JINR, Dubna (1974).
[58] V. V. Burov, V. K. Luk'yanov, and A. I. Titov, Fiz. Elem. Chastits At. Yadra **15**, 1249 (1984) [Sov. J. Part. Nucl. **15**, 558 (1984)].
[59] A. B. Kaĭdalov, in *Proc. of the 10th Physics School of the Institute of Theoretical and Experimental Physics*, No. 2 [in Russian] (Énergoizdat, Moscow, 1983), p. 3.
[60] A. V. Efremov, A. B. Kaĭdalov, V. T. Kim *et al.*, Yad. Fiz. **47**, 1364 (1988) [Sov. J. Nucl. Phys. **47**, 868 (1988)].
[61] A. V. Efremov, Preprint R2-87-762 [in Russian], JINR, Dubna (1987).
[62] L. M. Anderson *et al.*, Preprint 14-330, LBL, Berkeley (1982).
[63] E. A. Strokovsky *et al.*, in *Proc. of the Few Body Conference* (Australia, 1991).
[64] R. F. Owens and J. D. Kimel, Phys. Rev. D **18**, 3313 (1978).
[65] A. V. Efremov and E. A. Bondarchenko, Preprint E2-84-124, JINR, Dubna (1984).
[66] W. P. Shutz *et al.*, Phys. Rev. Lett. **38**, 259 (1977).
[67] R. V. Reid, Ann. Phys. (N.Y.) **50**, 411 (1968).
[68] M. Lacombe *et al.*, Phys. Lett. **151B**, 139 (1981).
[69] I. S. Shapiro, Dokl. Akad. Nauk SSSR **106**, 647 (1956) [Sov. Phys. Dokl. **1**, 91 (1956)].
[70] V. G. Kadyshevsky, R. M. Mir-Kasimov, and N. V. Skachkov, Nuovo Cimento **A55**, 233 (1968).
[71] L. G. Dakhno and N. N. Nikolaev, Nucl. Phys. **A436**, 653 (1985).
[72] M. Lacombe, B. Loiseau, J. M. Richard *et al.*, Phys. Rev. C **21**, 861 (1980).
[73] M. Chemtov, Nucl. Phys. **A34**, 387 (1979).
[74] V. B. Kopeliovich, Phys. Rep. **139**, 51 (1986).
[75] A. M. Baldin *et al.*, Communication R1-11186 [in Russian], JINR, Dubna (1977).
[76] S. V. Dzshemuchadze *et al.*, *Proposal for Deuteron Disintegration Study at COSY in Exclusive Experiments with Polarized Protons and Deuterons* (Dubna–Jülich, 1991).

Translated by Julian B. Babour